Supplement of Geosci. Model Dev., 10, 1521–1548, 2017
http://www.geosci-model-dev.net/10/1521/2017/
doi:10.5194/gmd-10-1521-2017-supplement

Geoscientific Model Development
Open Access
EGU

Supplement of

Collection/aggregation algorithms in Lagrangian cloud microphysical models: rigorous evaluation in box model simulations

Simon Unterstrasser et al.

Correspondence to: Simon Unterstrasser (simon.unterstrasser@dlr.de)

Contents

1 Introduction

This document contains a systematic collection of figures. Any figure is a 4x1 panel showing the SIP number, droplet number and the second and third moment of the droplet mass distribution. All quantities are averages over 50 instances. Blocks 1, 2 and 3 show simulation results of the Remapping Algorithm (RMA), the Average Impact Algorithm (AIM) and the All-Or-Nothing algorithm (AON), respectively. Each block is divided into sections dealing with a specific kernel (Hall, Long and Golovin). The complete structure of the document becomes clear from looking at the table of contents which lists all presented sensitivity studies.
All plots showing the sensitivity to dt use the colour and linestyle coding as given in the first row of the Table 1.
All plots showing the sensitivity to κ use the colour coding as given in the second row of the Table 1.
All plots showing the sensitivity to N_{SIP} use the colour coding as given in the second row of the Table 1.
A specific plot does not necessarily show curves for all parameter values listed in Table 1. Moreover, the y-scale runs in all N_{SIP}-plots (top row) from 0 to 600 (and sometimes t0 400) and the plots miss to show simulations with larger N_{SIP}. It occurs quite often that several curves overlap and it is not clear which curves are actually not shown or which are just hidden by other curves. In the case, where κ or N_{SIP} is varied, the N_{SIP}-plot helps to see which curves are plotted. For other sensitivities, it is most often not evident which parameter values are actually shown.

Table 1: Colour coding for the various sensitivity simulations series. By default, the linestyle is solid. For the values listed with a *-symbol, dotted curves are used.

dt	0.01	0.05	0.1	0.5	1	2	5	10	20*	50*	100*	200*
κ	5	10	20	40	60	100	200	400				
N_{SIP}	40	80	160	240	400	800	1600					
η (RMA)	10^{-5}	10^{-6}	10^{-7}	10^{-8}	10^{-10}	10^{-15}						
η (AIM,AON)	10^{-6}	10^{-7}	10^{-8}	10^{-9}	10^{-12}	10^{-15}	10^{-20}					
α_{low}	-5	-7	-9	-13								

2 Simulation Results of Remapping Algorithm (RMA)

Block 2 displays RMA simulation results for the Golovin and Long kernel (no Hall simulations are included in this document).
The default settings are $\eta = 10^{-8}$ (weak threshold) and $r_{critmin} = 1.6\,\mu$m.
For Golovin RMA simulations the default is: $dt = 1\,\mathrm{s}, \kappa = 40$ and the algorithm version without Reduction Limiter.
For Long RMA simulations the default is: $dt = 0.1\,\mathrm{s}, \kappa = 10$ and the algorithm version with Reduction Limiter.

For the algorithm with Reduction Limiter the parameter $\tilde{\gamma} = 0.1$.

2.1 Golovin Kernel (RMA)

The following sections show Golovin RMA results for the regular algorithm, the version with Reduction Limiter, the version with Update on the Fly (OTF_s, starting with the smallest SIPs) and the version with Update on the Fly (OTF_l, starting with the largest SIPs)

2.1.1 Golovin Kernel (RMA), regular RMA version

2.1.1.1 Variation of dt and κ

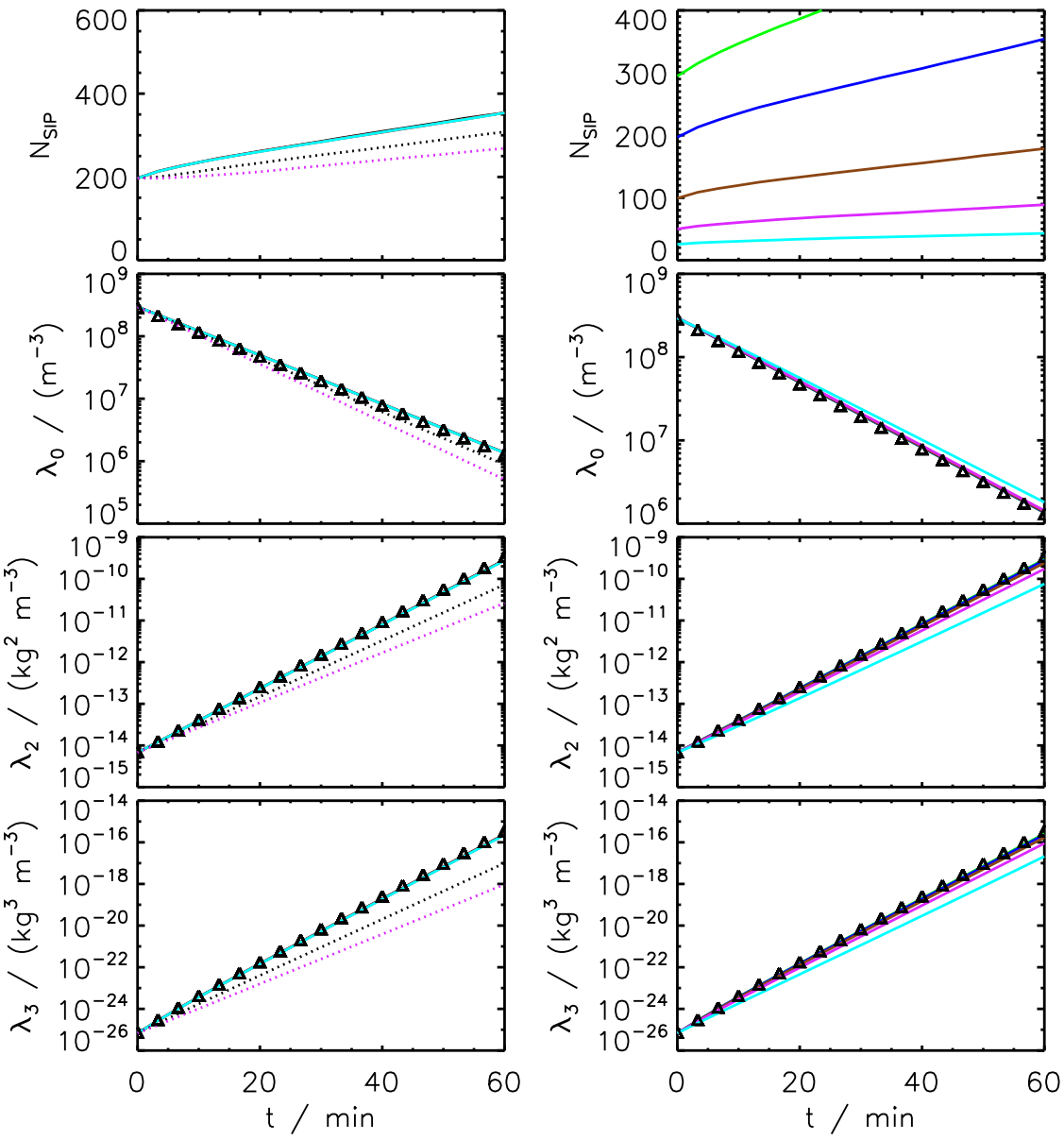

Figure 1: GOL RMA: Variation of time step dt (left) and bin resolution κ (right).

2.1.1.2 Variation of η

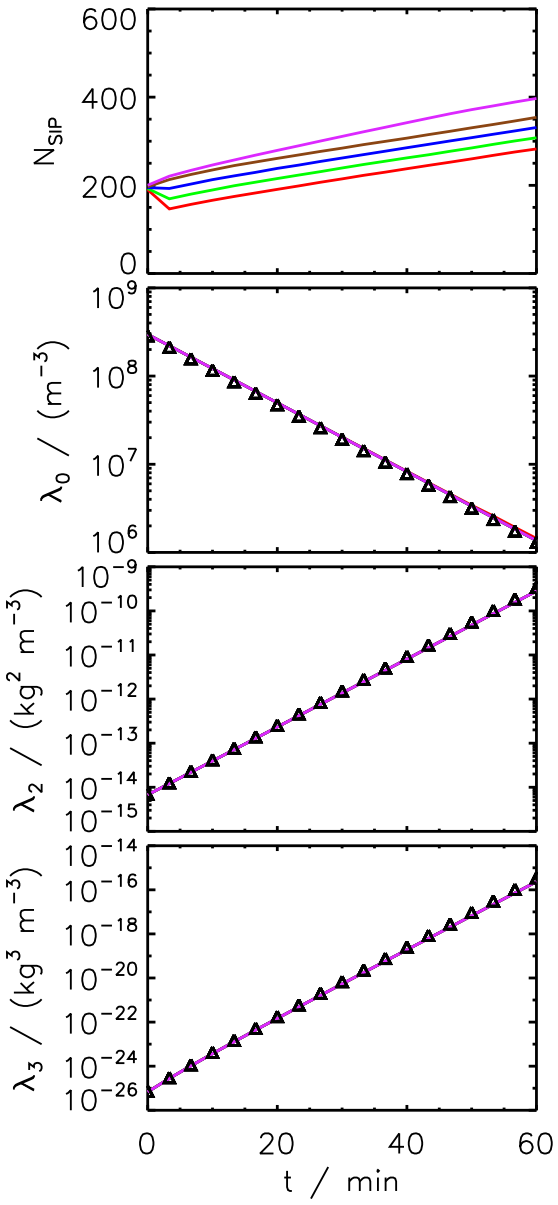

Figure 2: GOL RMA: Variation of (weak) threshold η.

2.1.1.3 Strict threshold, variation of η No SIPs are generated from bins with $M_{bin,l} < M_{critmin} = \eta\lambda_1$. This is the only plot in the document, where λ_1 is shown. For too large η, mass is not conserved.

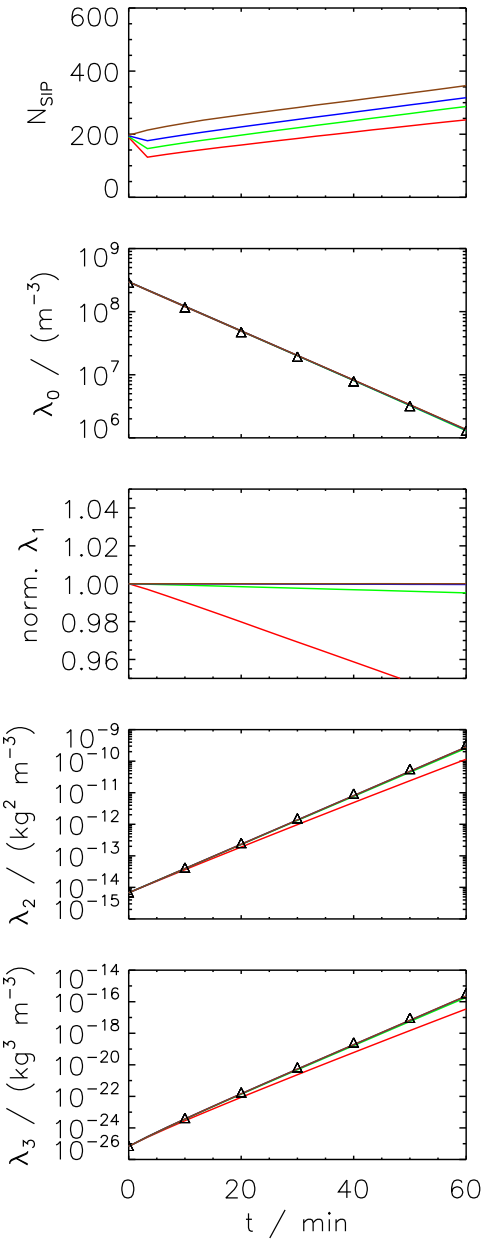

Figure 3: GOL RMA: Variation of strict threshold η.

2.1.2 Golovin Kernel (RMA), RMA with Reduction Limiter

2.1.2.1 Variation of dt and κ

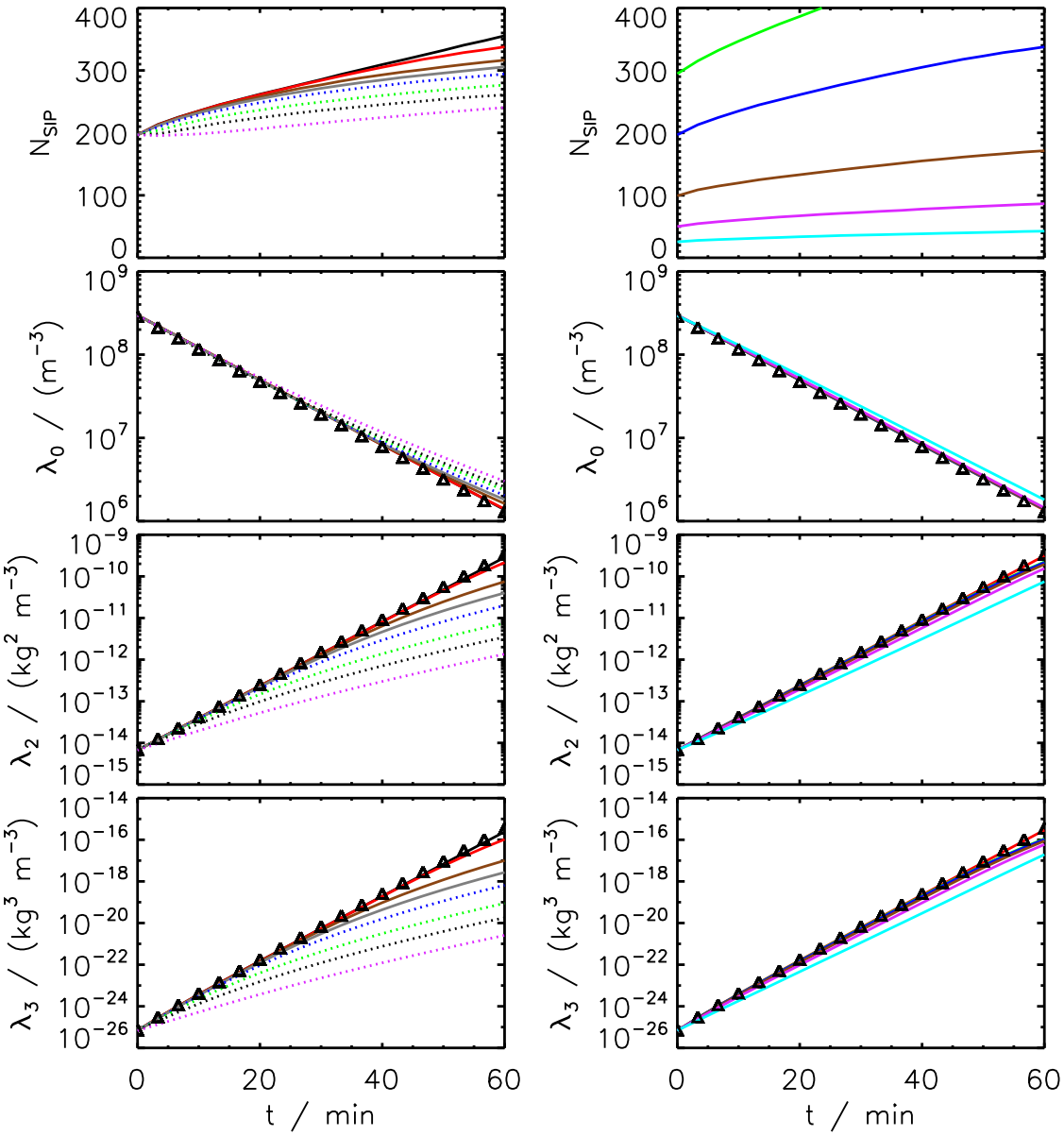

Figure 4: GOL RMA (with Reduction Limiter): Variation of time step dt (left) and bin resolution κ (right).

2.1.2.2 Variation of $r_{critmin}$ and η

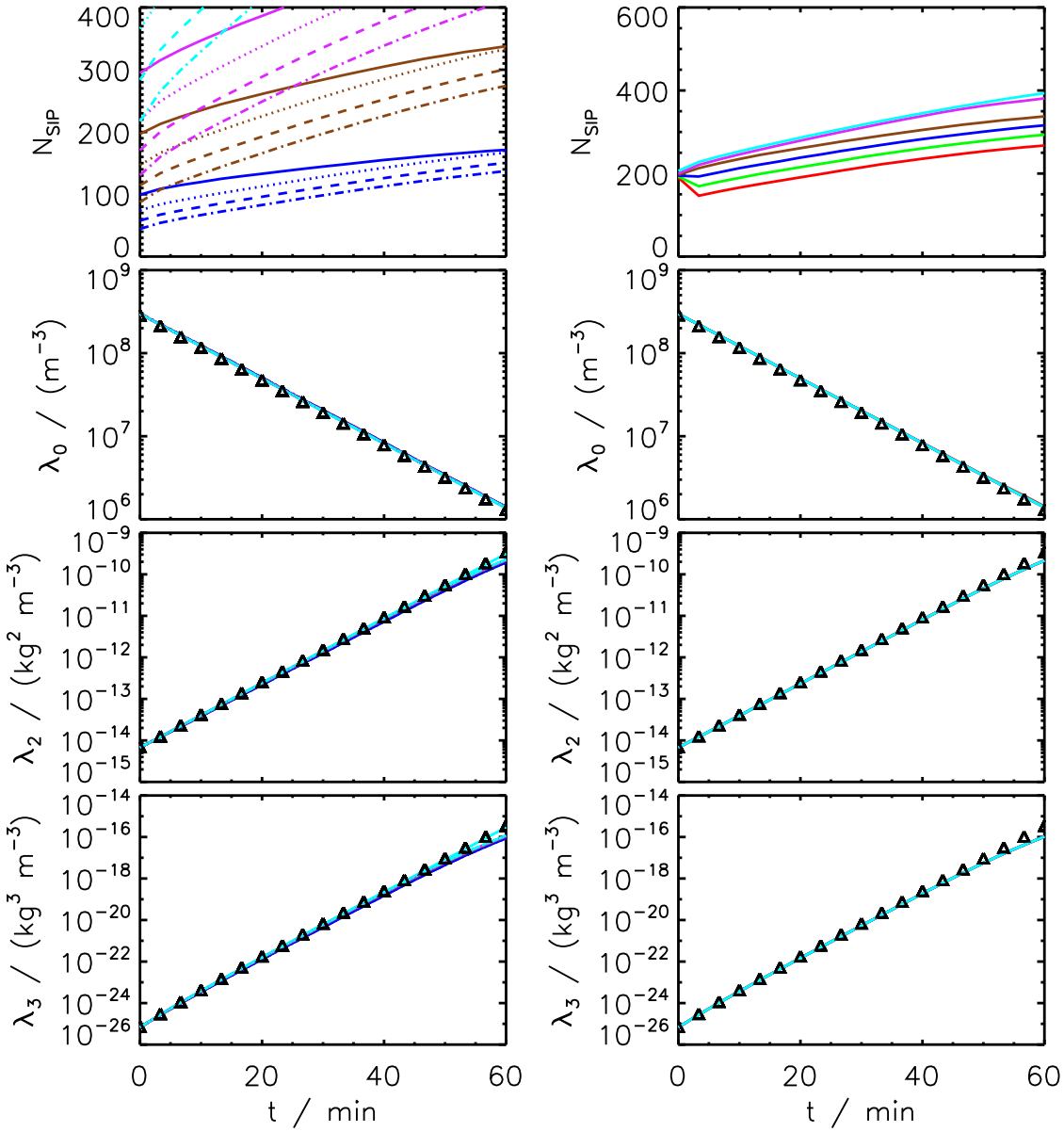

Figure 5: GOL RMA (with Reduction Limiter): Variation of $r_{critmin}$ (left). Colours indicate the κ-value and the linestyle the $r_{critmin}$-value: 0.6 μm (solid), 1.6 μm (dotted), 3.0 μm (dashed), 5.0 μm (dash-dotted). Variation of threshold η (right).

2.1.2.3 Variation of $\tilde{\gamma}$

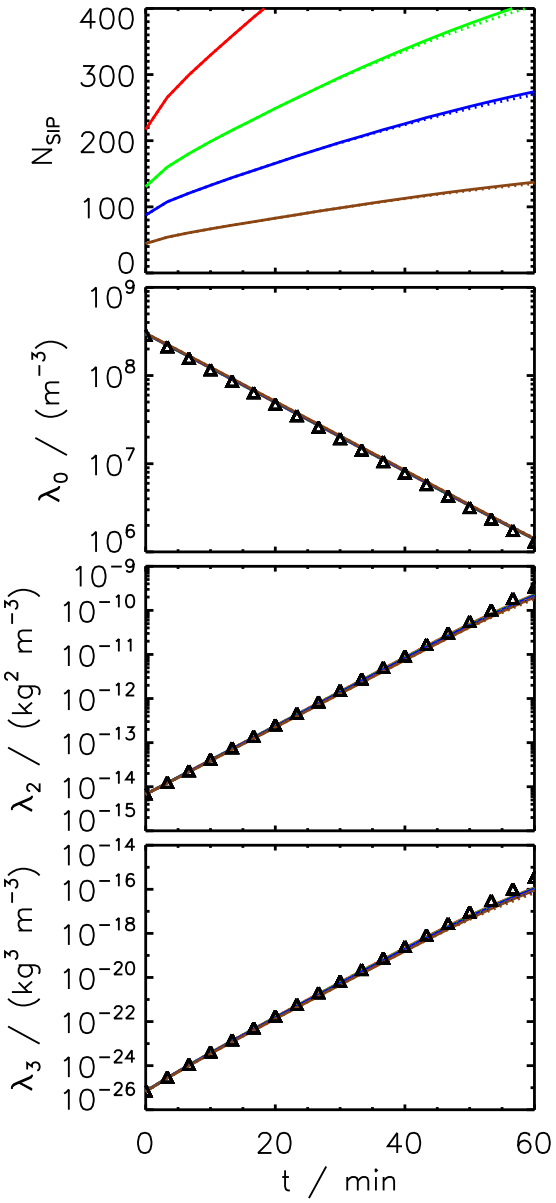

Figure 6: GOL RMA (with Reduction Limiter): two values of scaling factor $\tilde{\gamma}$ (default value 0.1 solid and value 0.5 dotted) for various κ.

2.1.3 Golovin Kernel (RMA), RMA with Update on the Fly OTF$_s$

2.1.3.1 Variation of dt and κ

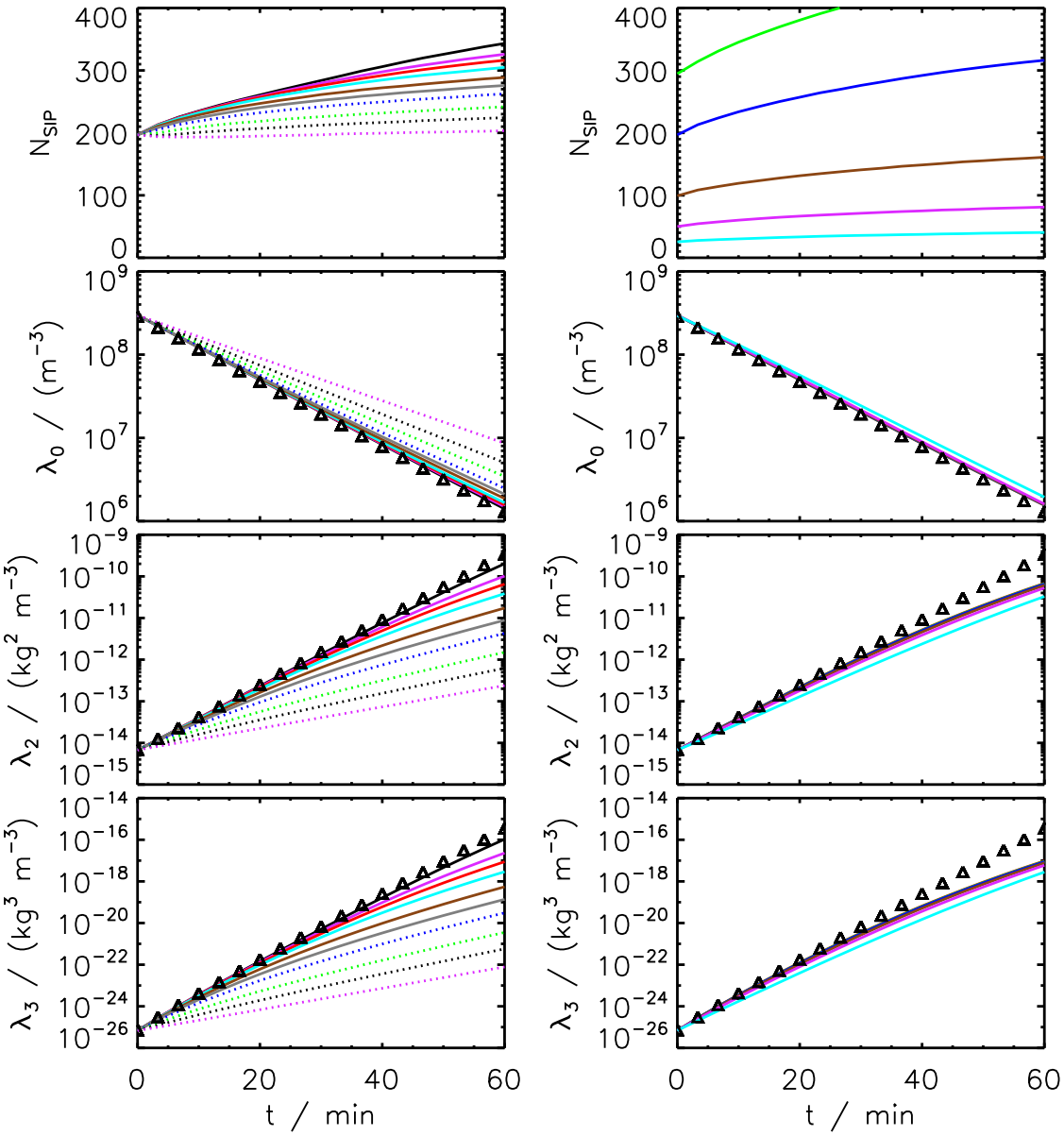

Figure 7: GOL RMA (with OTF$_s$): Variation of time step dt (left) and bin resolution κ (right).

2.1.4 Golovin Kernel (RMA), RMA with Update on the Fly OTF$_l$

2.1.4.1 Variation of dt and κ

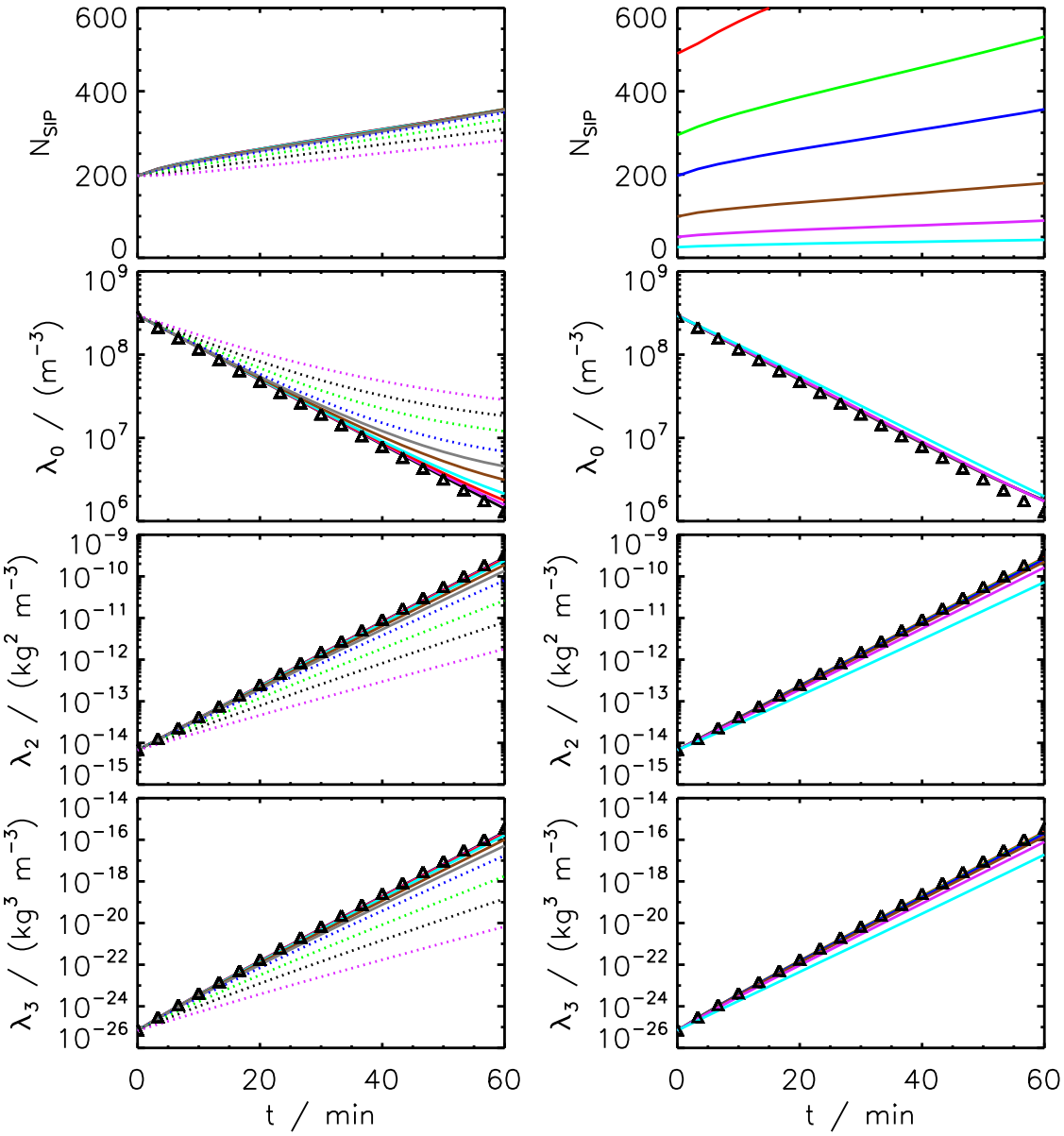

Figure 8: GOL RMA (with OTF$_l$): Variation of time step dt (left) and bin resolution κ (right).

2.2 Long Kernel (RMA)

The following sections show Long RMA results for the algorithm with Redcution Limiter and for the version with Update on the Fly (OTF_l, starting with the largest SIPs)

2.2.1 Long Kernel, RMA with Reduction Limiter

2.2.1.1 Variation of dt and κ

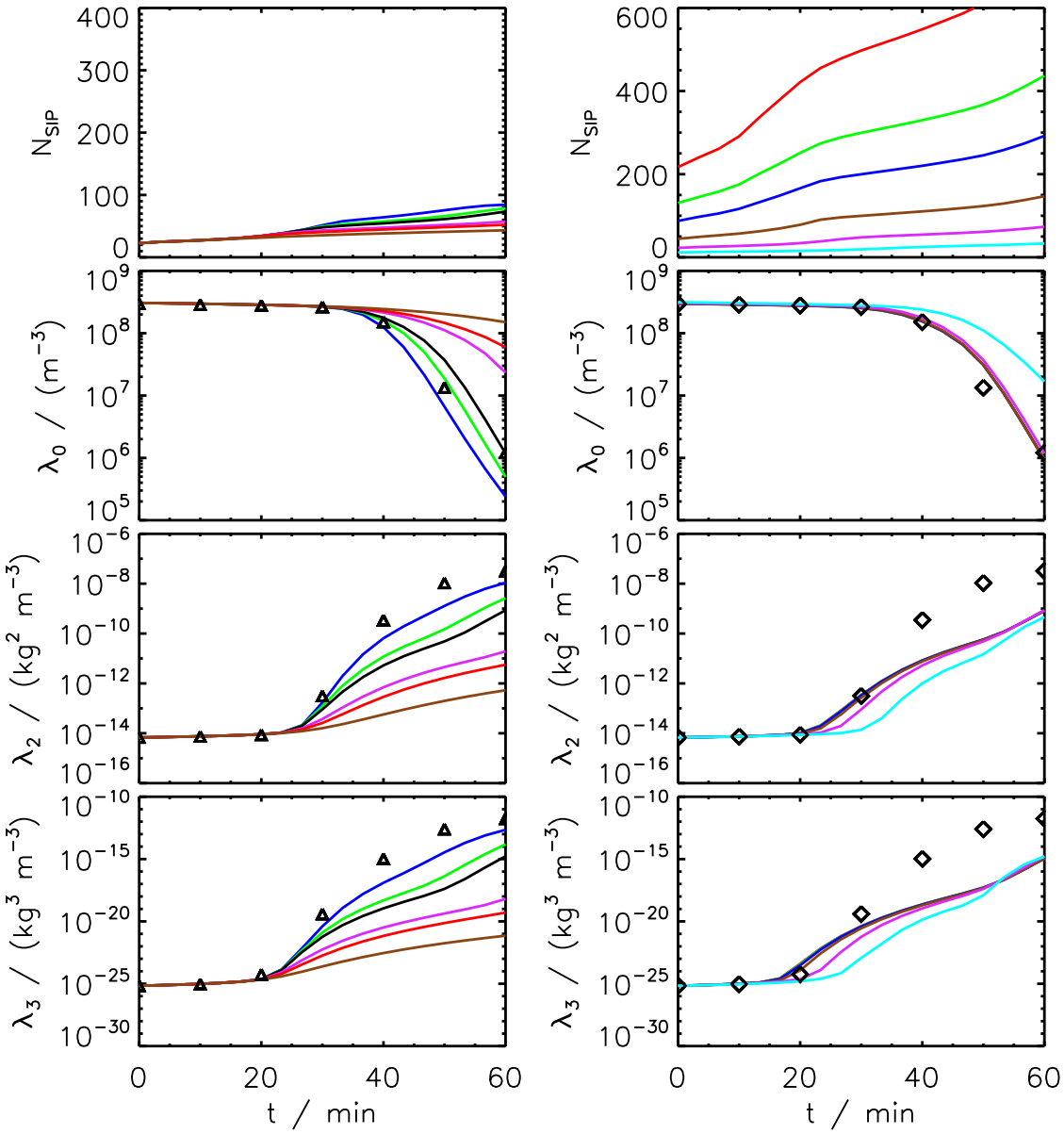

Figure 9: LONG RMA (with Reduction Limiter): Variation of time step dt (left) and bin resolution κ (right).

2.2.1.2 Variation of t_{init} and η

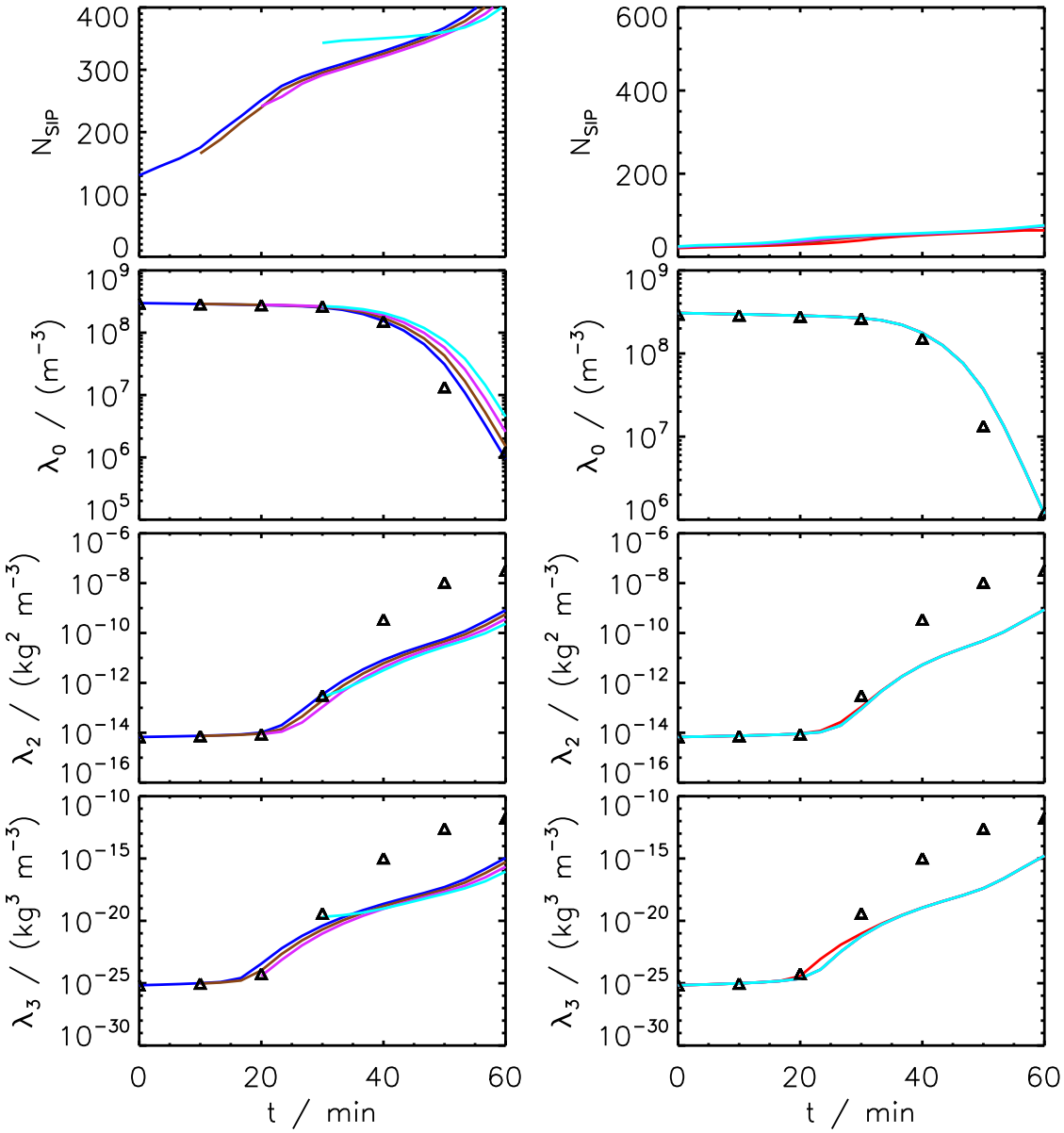

Figure 10: LONG RMA (with Reduction Limiter): Variation of t_{init} at $\kappa = 60$ (left). The colours are as follows: $t_{init}/\,\mathrm{min} = 0$ (blue), 10 (brown), 20 (magenta) and 30 (cyan). Variation of threshold η (right).

2.2.2 Long Kernel, RMA with Update on the Fly OTF$_l$

2.2.2.1 Variation of dt and κ

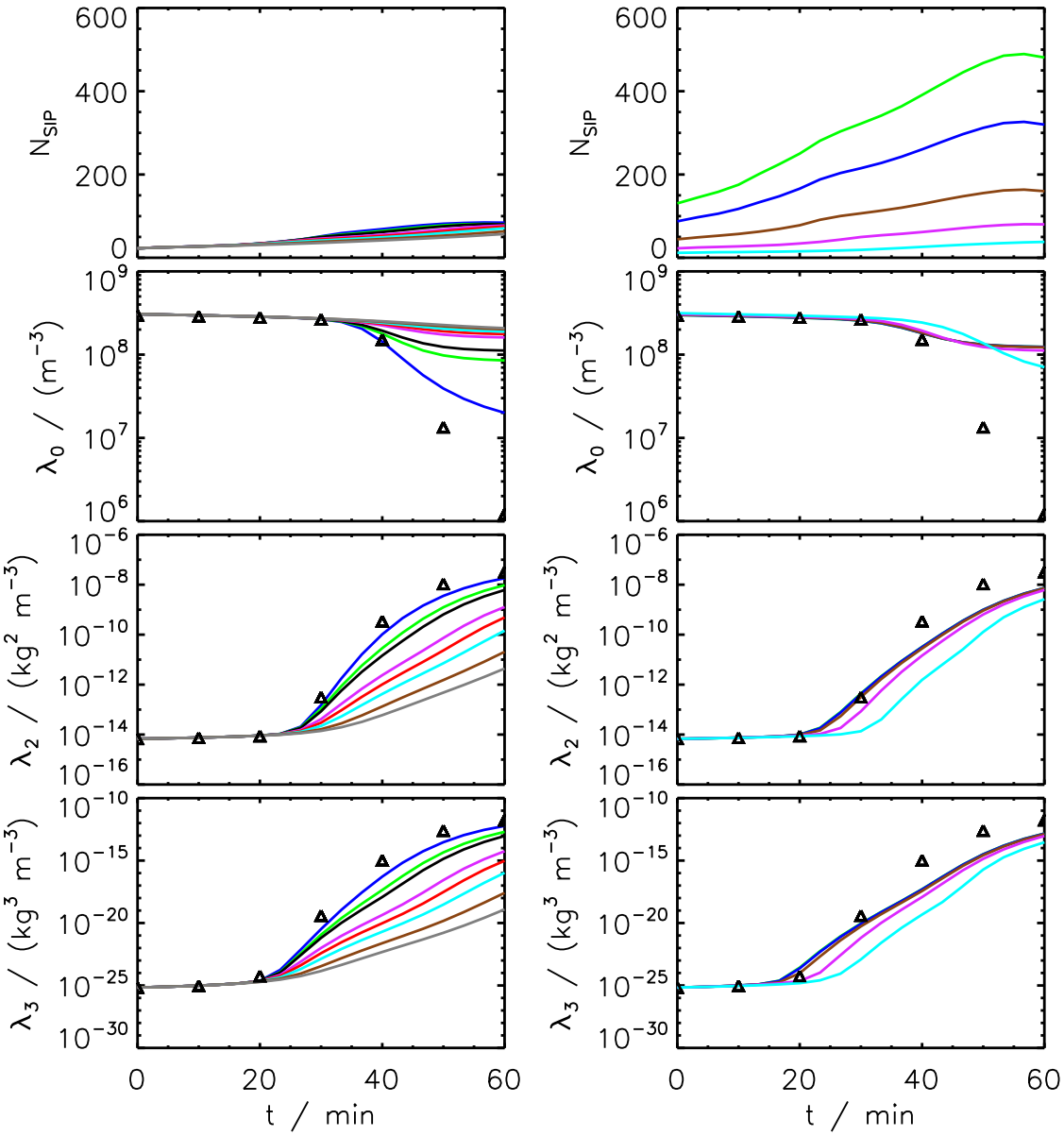

Figure 11: LONG RMA (with OTF$_l$): Variation of time step dt (left) and bin resolution κ (right).

3 Simulation Results of Average Impact Algorithm (AIM)

Block 3 displays AIM simulation results for the Golovin, Long and Hall kernel.
All AIM simulations use as default $dt = 10\,\mathrm{s}$.
The SingleSIP initialisation method uses as default $\kappa = 40, r_{critmin} = 0.6\,\mu\mathrm{m}$ and $\eta = 10^{-8}$ and is probabilistic.
The ν_{const} and ν_{draw} initialisation methods use as default $N_{SIP} = 160$.

3.1 Golovin Kernel (AIM)

The following sections show Golovin AIM results for three types of init methods.

3.1.1 Golovin Kernel (AIM), SingleSIP-init

3.1.1.1 Variation of dt and κ

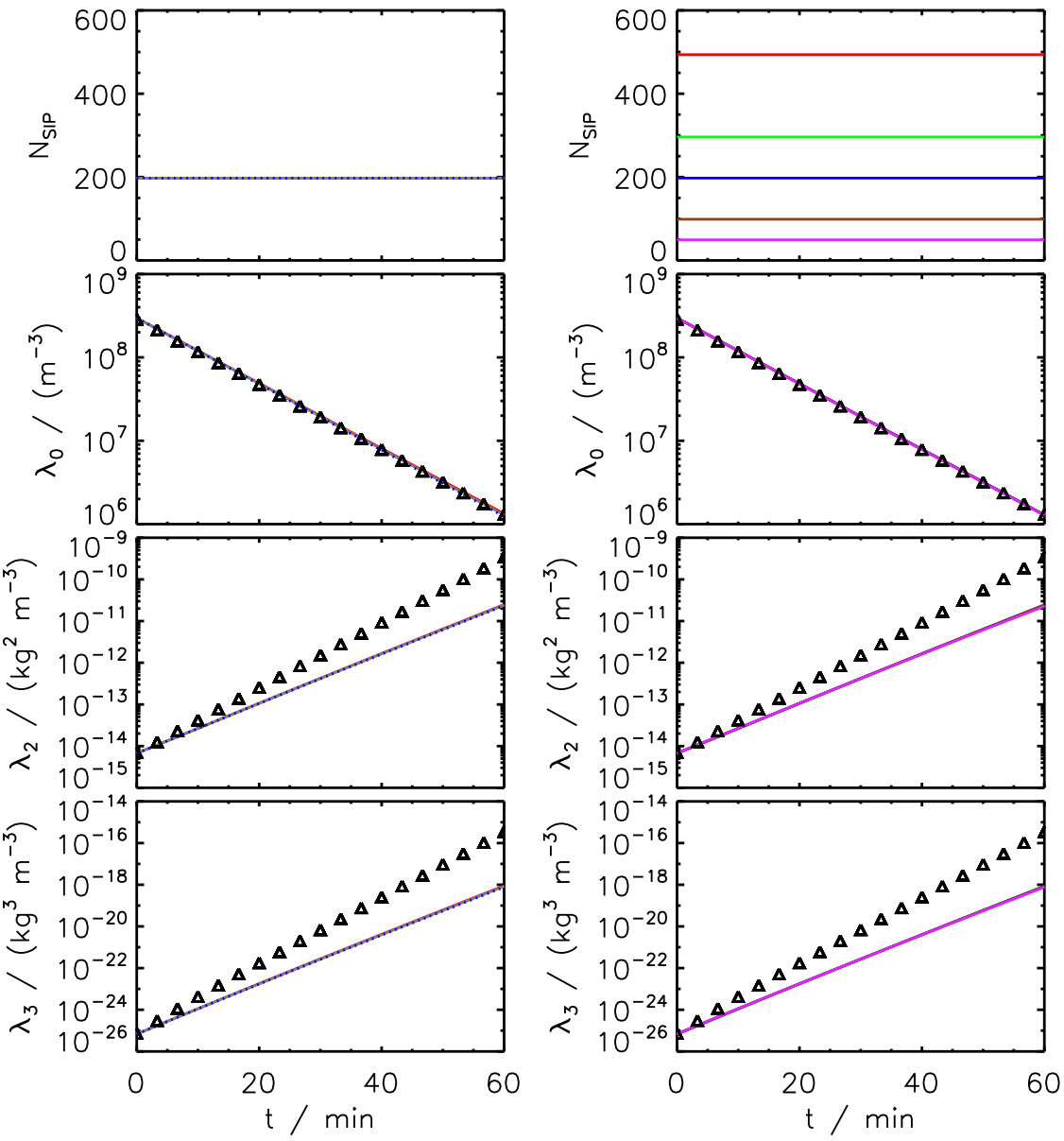

Figure 12: GOL AIM: Variation of time step dt (left) and bin resolution κ (right).

3.1.2 Golovin Kernel (AIM), ν_{const}-init

3.1.2.1 Variation of N_{SIP}

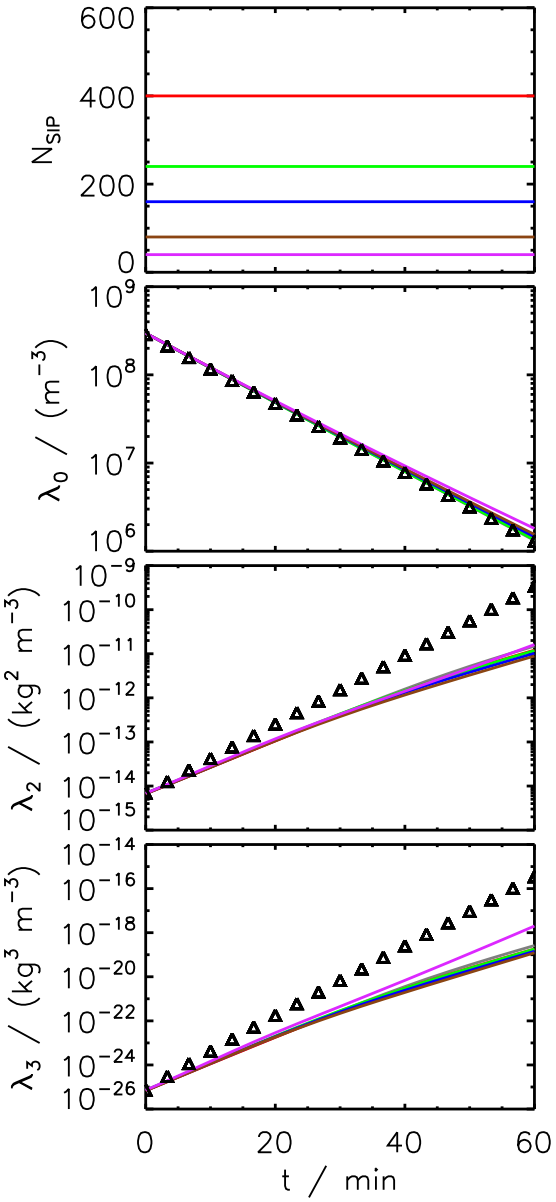

Figure 13: GOL AIM: Variation of SIP number N_{SIP}.

3.1.3 Golovin Kernel (AIM), ν_{draw}-init

3.1.3.1 Variation of N_{SIP}

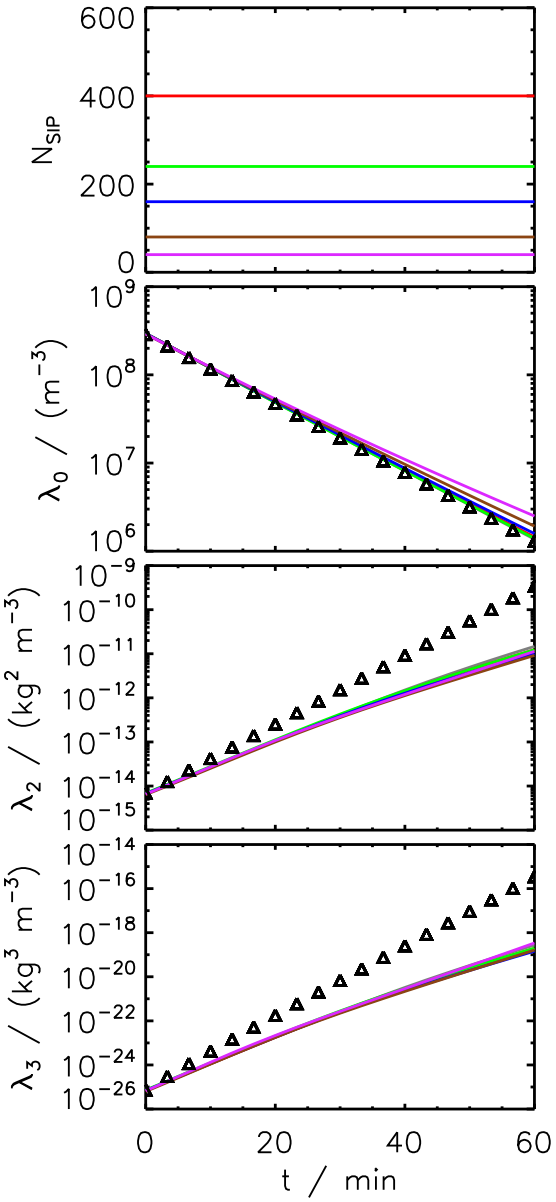

Figure 14: GOL AIM: Variation of SIP number N_{SIP}.

3.2 Long Kernel (AIM)

The following sections show Long AIM results for five types of init methods.

3.2.1 Long Kernel (AIM), SingleSIP-init

3.2.1.1 Variation of dt and κ

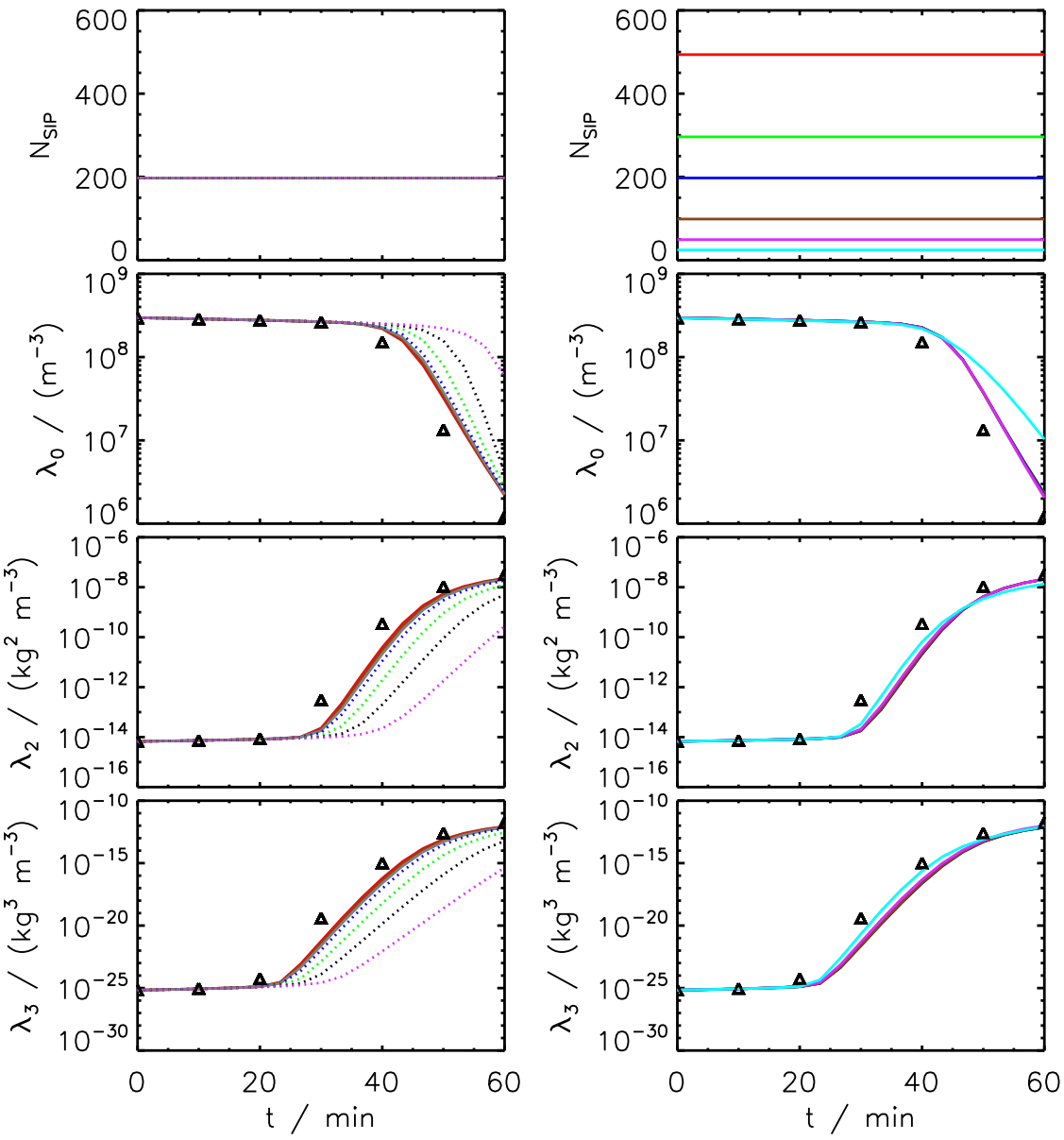

Figure 15: LONG AIM: Variation of time step dt (left) and bin resolution κ (right).

3.2.1.2 Variation of η

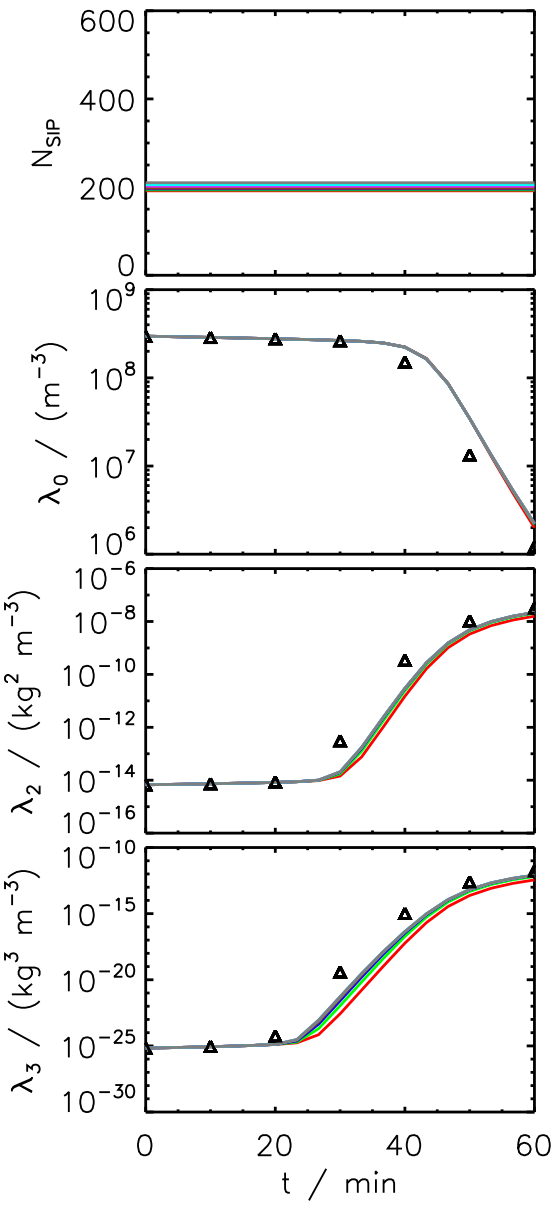

Figure 16: LONG AIM: Variation of threshold η.

3.2.1.3 Variation of $r_{critmin}$

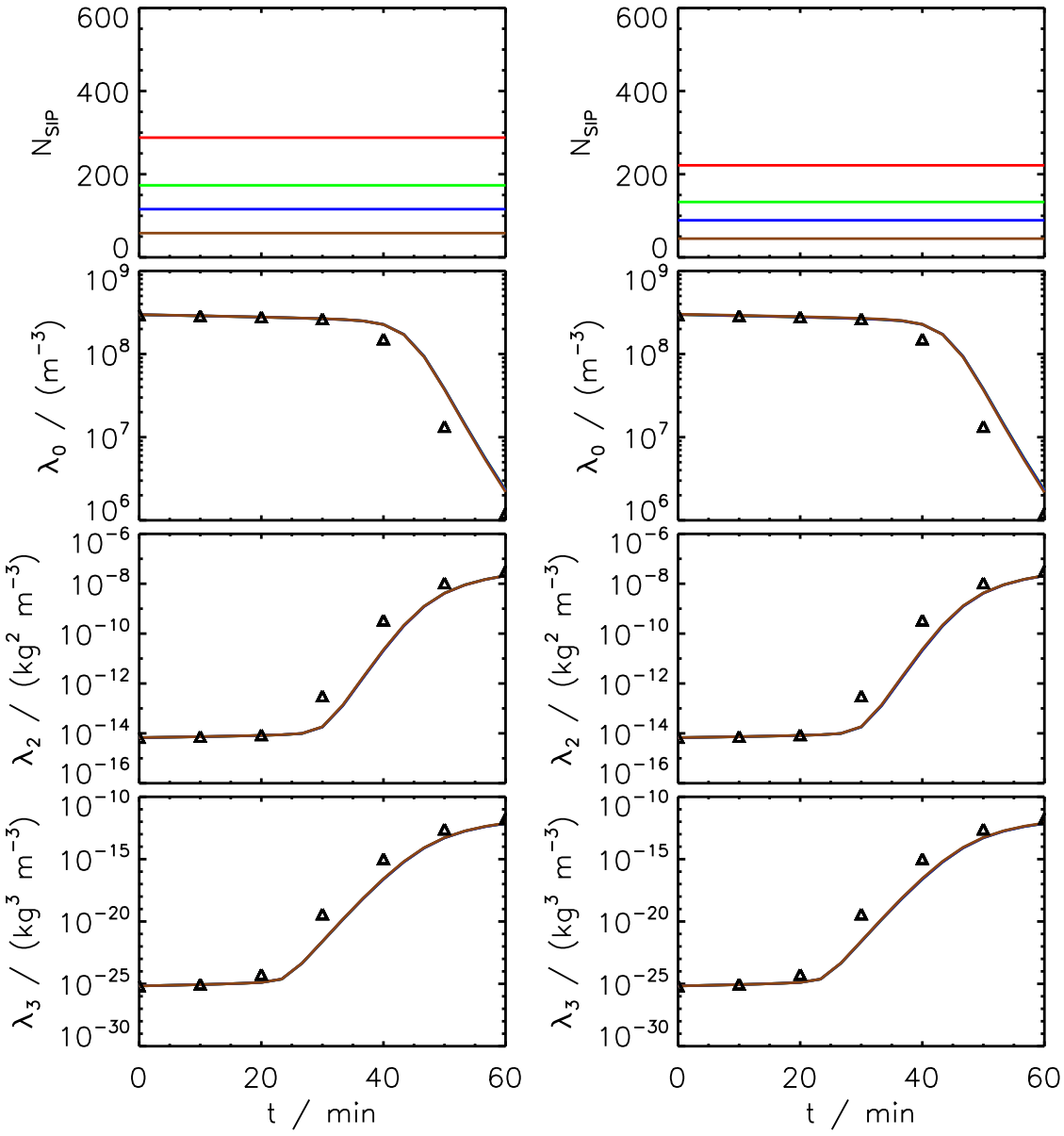

Figure 17: LONG AIM: Variation of bin resolution κ at $r_{critmin} = 3.0\,\mu$m (left) and $5.0\,\mu$m (right).

3.2.1.4 Variation of t_{init}

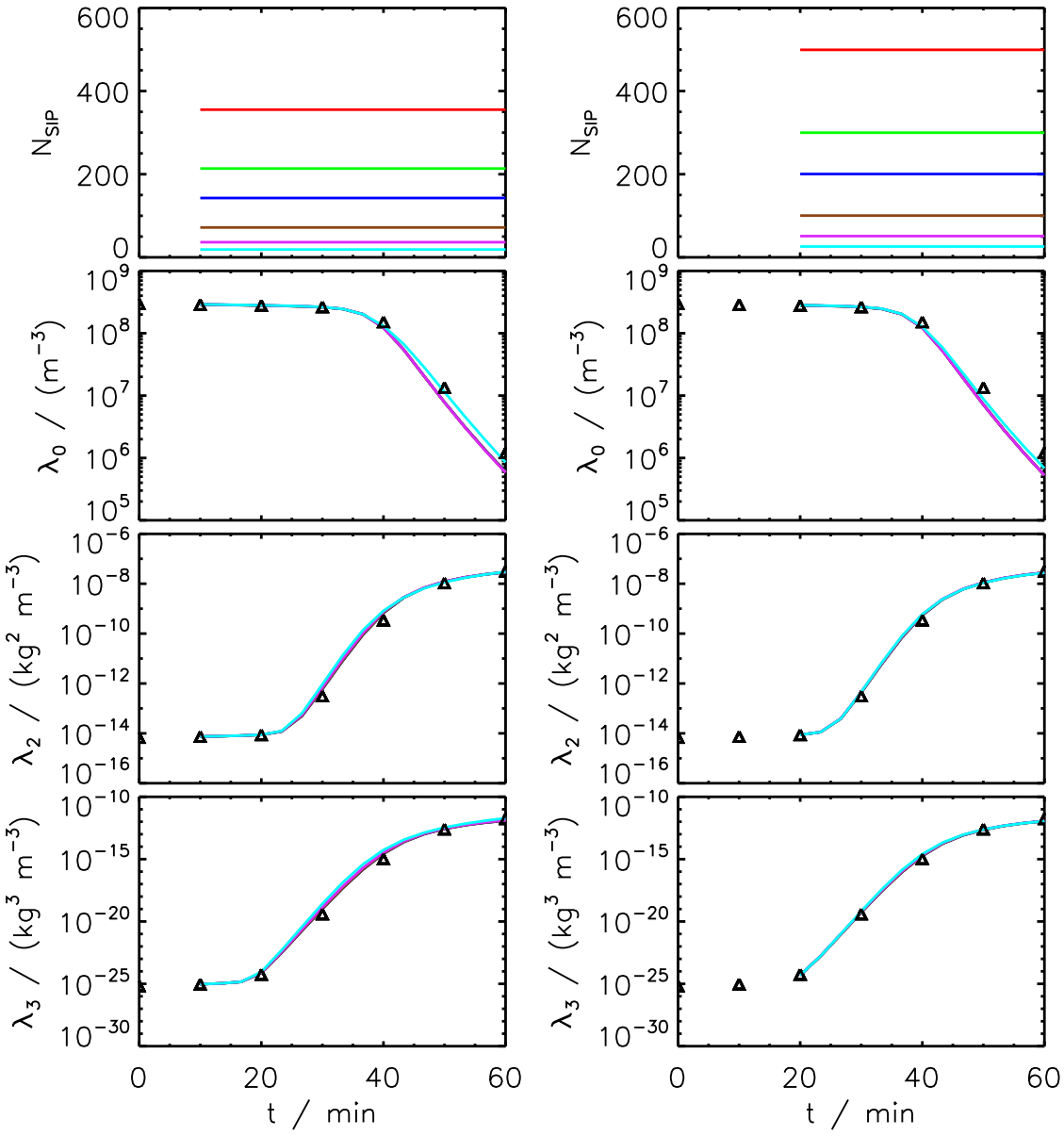

Figure 18: LONG AIM: Variation of bin resolution κ at $t_{init} = 10\,\text{min}$ (left) and $20\,\text{min}$ (right).

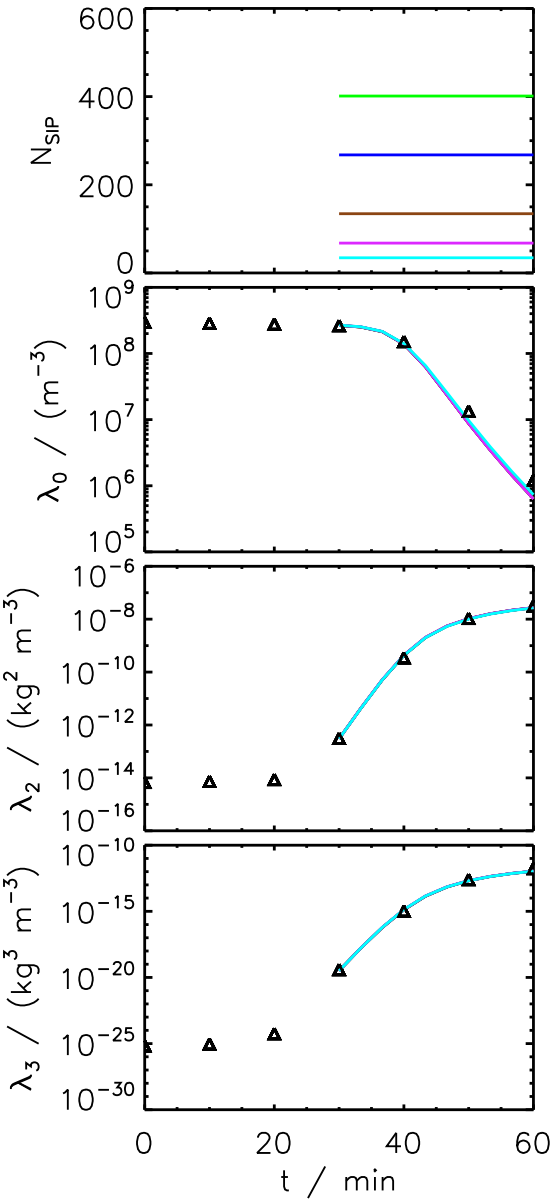

Figure 19: LONG AIM: Variation of bin resolution κ at $t_{init} = 30\,\text{min}$.

3.2.2 Long Kernel (AIM), ν_{const}-init

3.2.2.1 Variation of dt and N_{SIP}

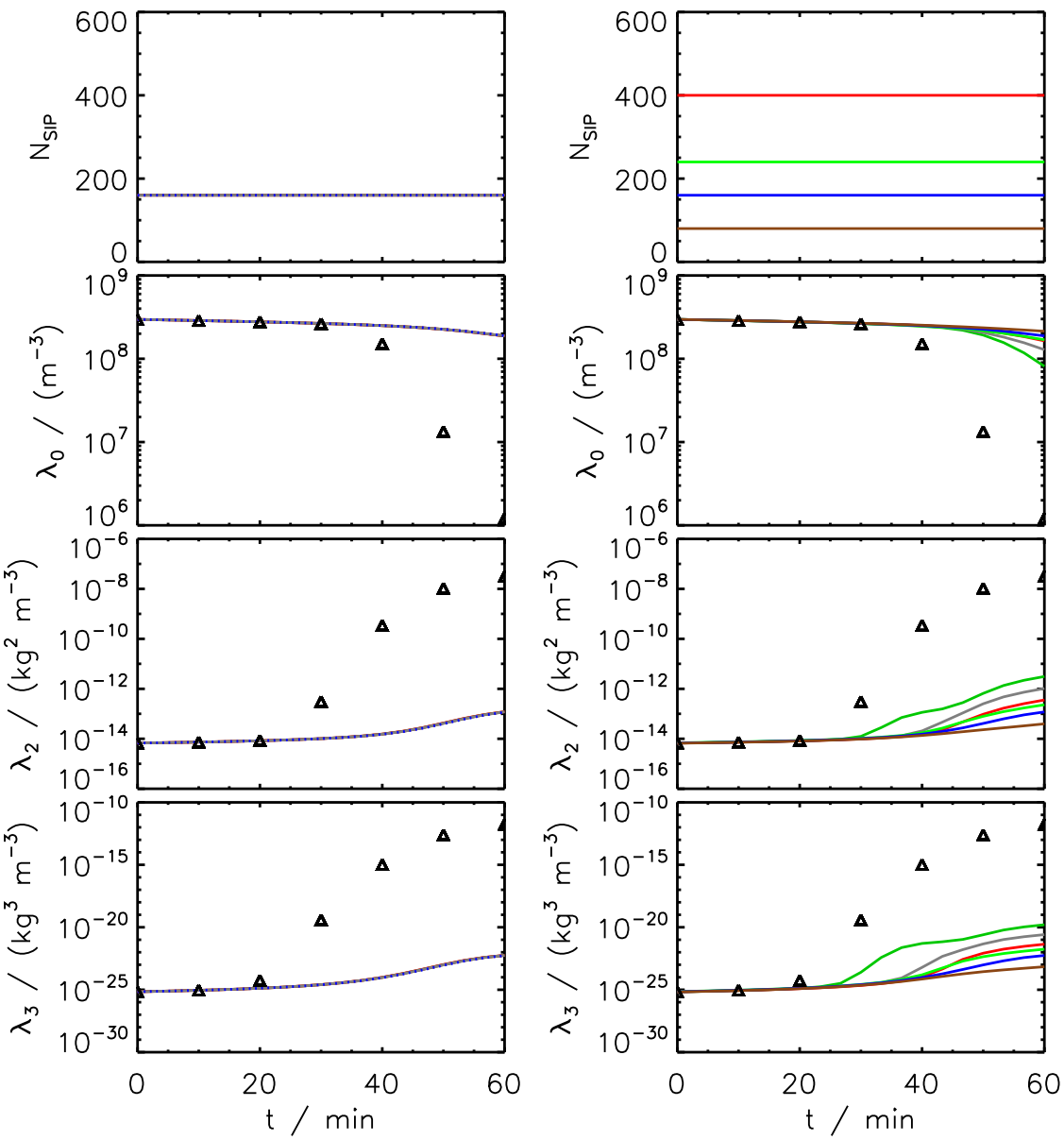

Figure 20: LONG AIM: Variation of time step dt and SIP number N_{SIP}.

3.2.3 Long Kernel (AIM), ν_{draw}-init

3.2.3.1 Variation of dt and N_{SIP}

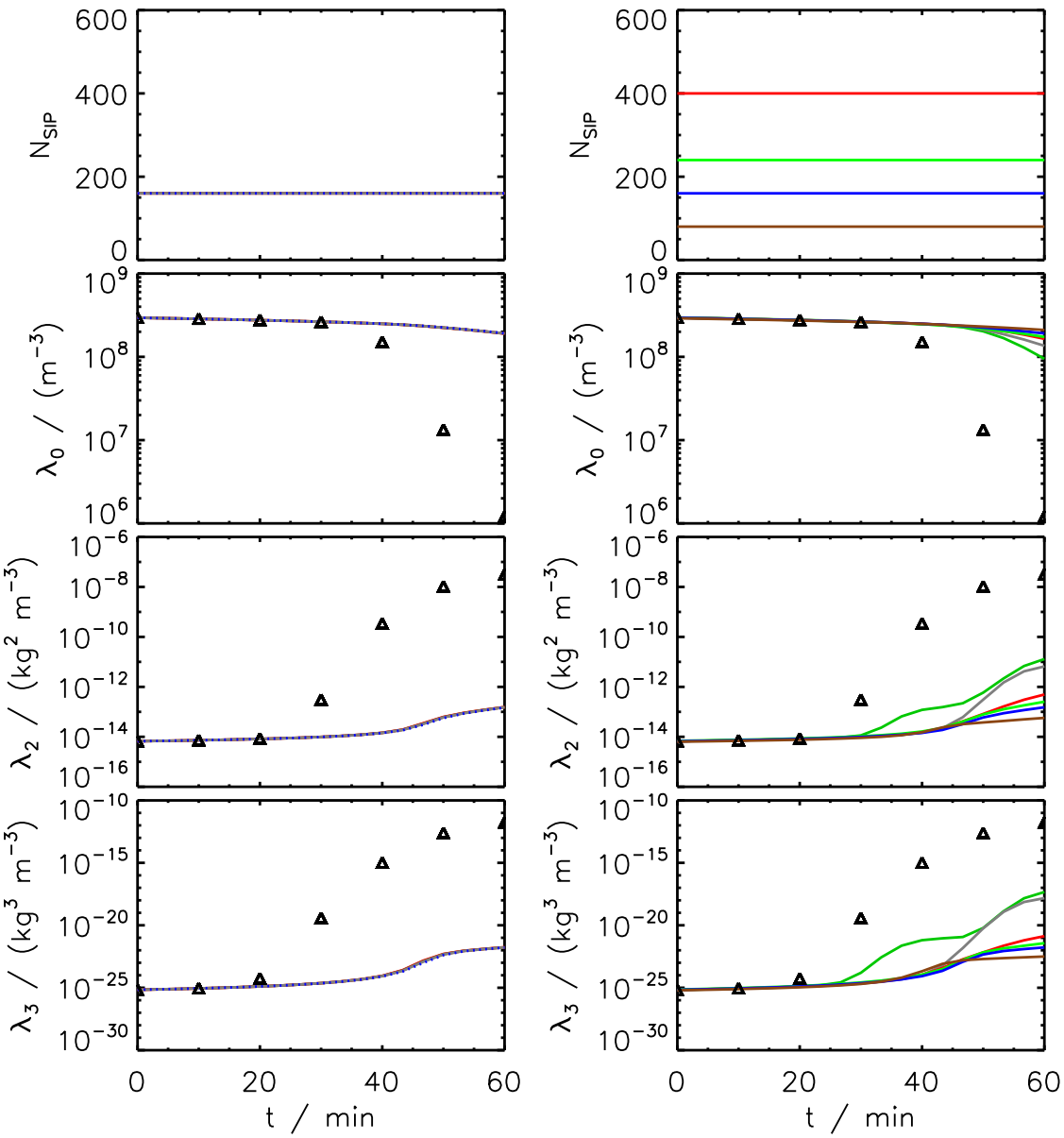

Figure 21: LONG AIM: Variation of time step dt and SIP number N_{SIP}.

3.2.4 Long Kernel (AIM), $\nu_{random,rs}$-init

3.2.4.1 Variation of dt and α_{low}

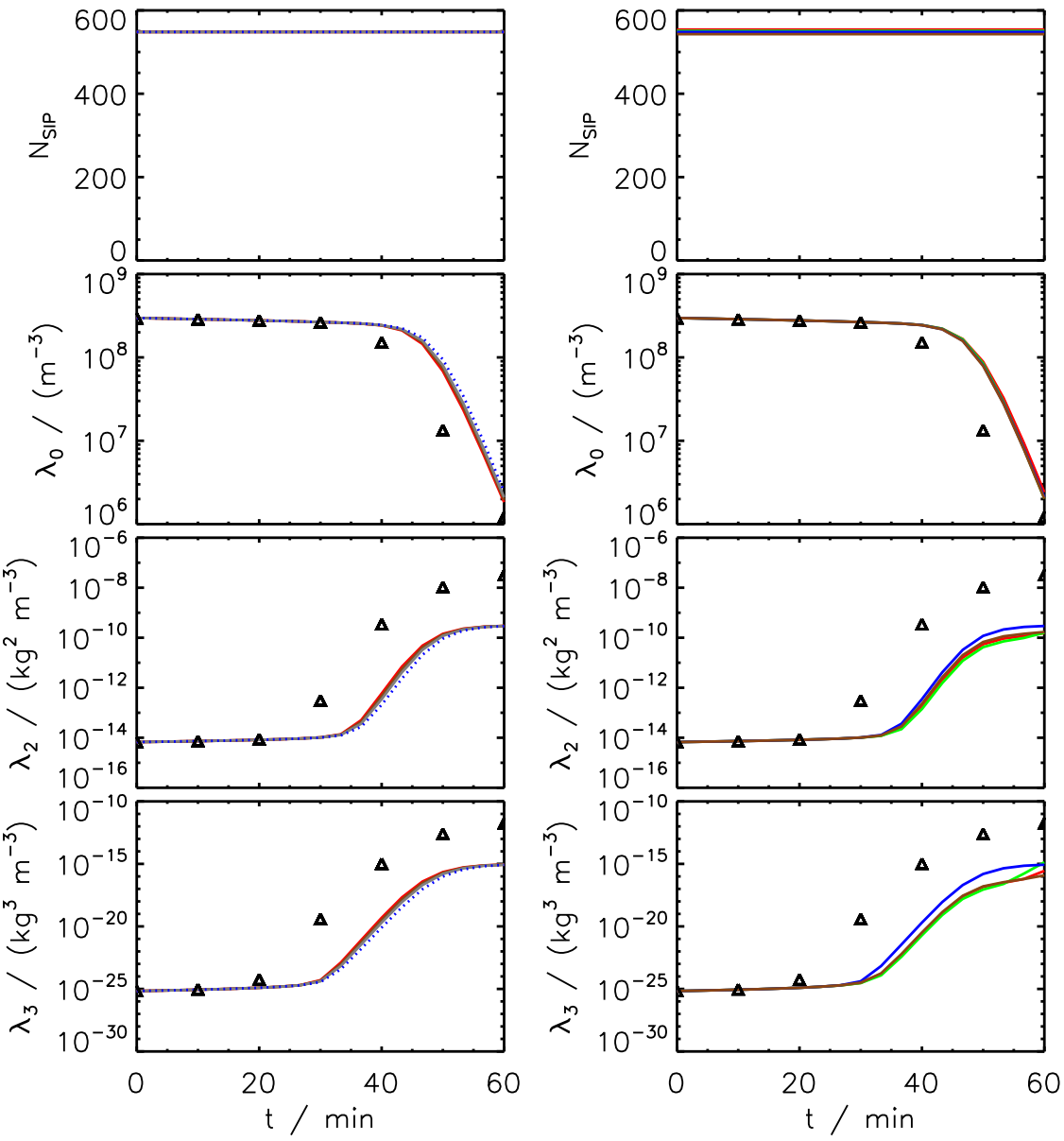

Figure 22: LONG AIM: Variation of time step dt (left) and lower threshold α_{low} (right).

3.2.5 Long Kernel (AIM), $\nu_{random,lb}$-init

3.2.5.1 Variation of dt and α_{low}

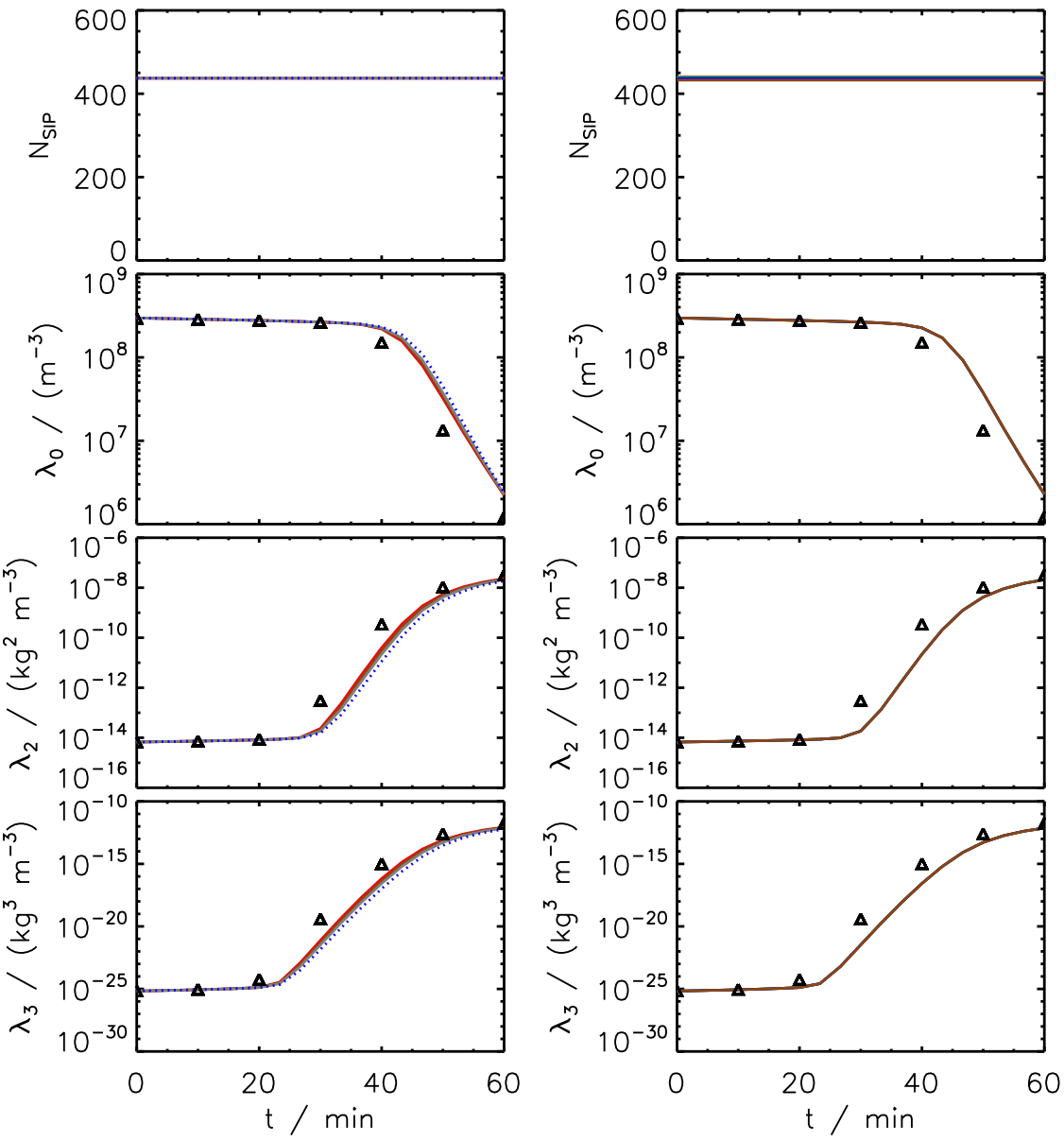

Figure 23: LONG AIM: Variation of time step dt(left) and lower threshold α_{low} (right).

3.3 Hall Kernel (AIM)

The following section show Hall AIM results for the SingleSIP init method.

3.3.1 Hall Kernel (AIM), SingleSIP-init

3.3.1.1 Variation of dt and κ

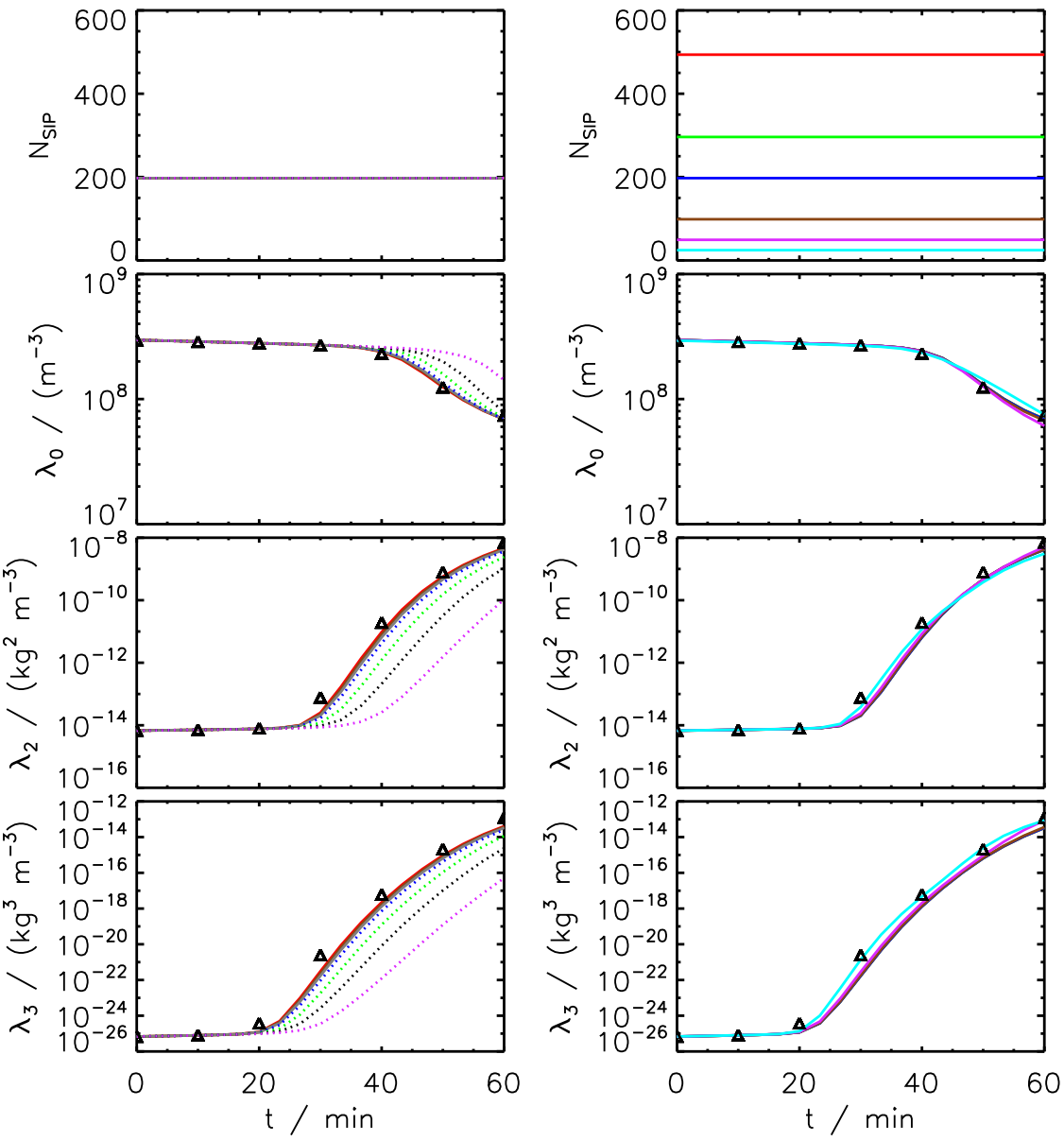

Figure 24: HALL AIM: Variation of time step dt (left) and bin resolution κ (right).

4 Simulation Results of All-or-Nothing Algorithm (AON)

Block 4 displays AON simulation results for the Golovin, Long and Hall kernel. Additionally, simulations with a "constant efficiency" kernel are included.
All AON simulations use as default $dt = 10\,\mathrm{s}$.
The SingleSIP initialisation method uses as default $\kappa = 40, r_{critmin} = 0.6\,\mu\mathrm{m}$ and $\eta = 10^{-8}$ and is probabilistic.
The ν_{const} and ν_{draw} initialisation methods use as default $N_{SIP} = 160$. For equal-weights collections (basically occurs only if ν_{const} init is used), equal splitting ($\xi = 0.5$) is applied as default.

4.1 Golovin Kernel (AON)

The following sections show Golovin AON results for three types of init methods and two variants of the SingleSIP-init method (change of $r_{critmin}$ and deterministic version).

4.1.1 Golovin Kernel (AON), SingleSIP-init

4.1.1.1 Variation of dt and κ

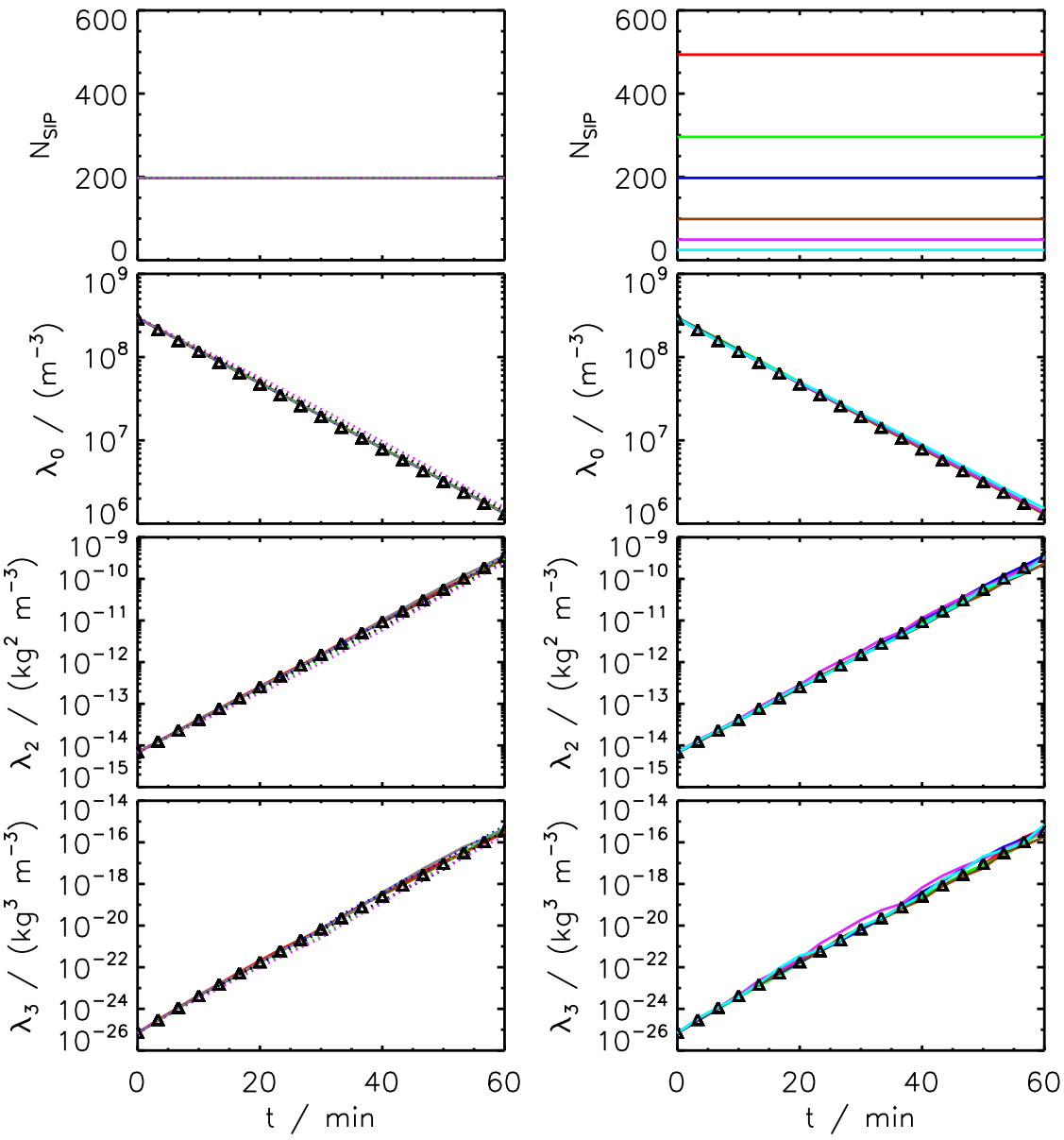

Figure 25: GOL AON: Variation of time step dt (left) and bin resolution κ (right).

4.1.2 Golovin Kernel (AON), SingleSIP-init with $r_{critmin} = 1.6\,\mu$m

4.1.2.1 Variation of dt and κ

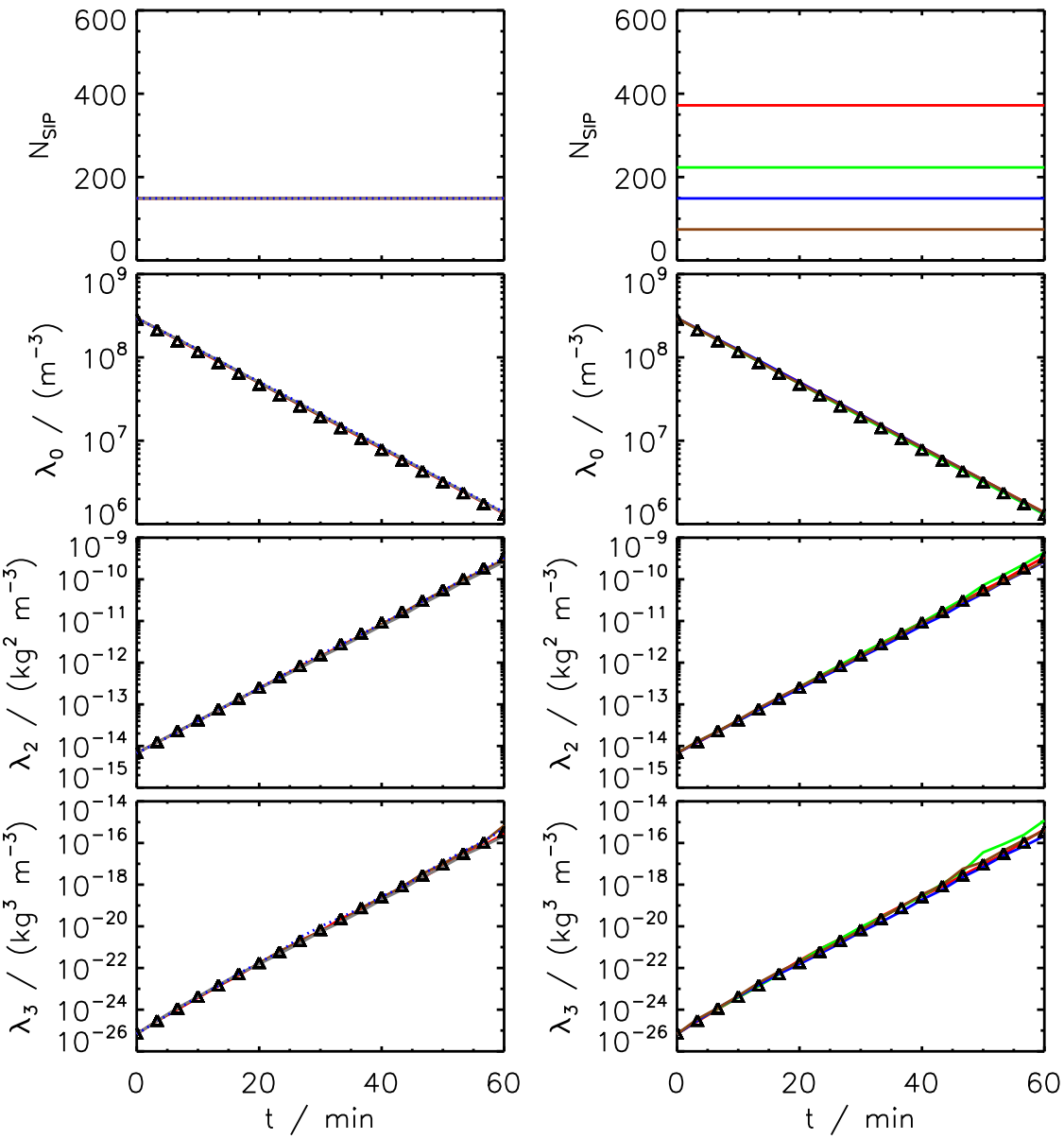

Figure 26: GOL AON: Variation of time step dt (left) and bin resolution κ (right).

4.1.3 Golovin Kernel (AON), Deterministic SingleSIP-init

4.1.3.1 Variation of dt and κ

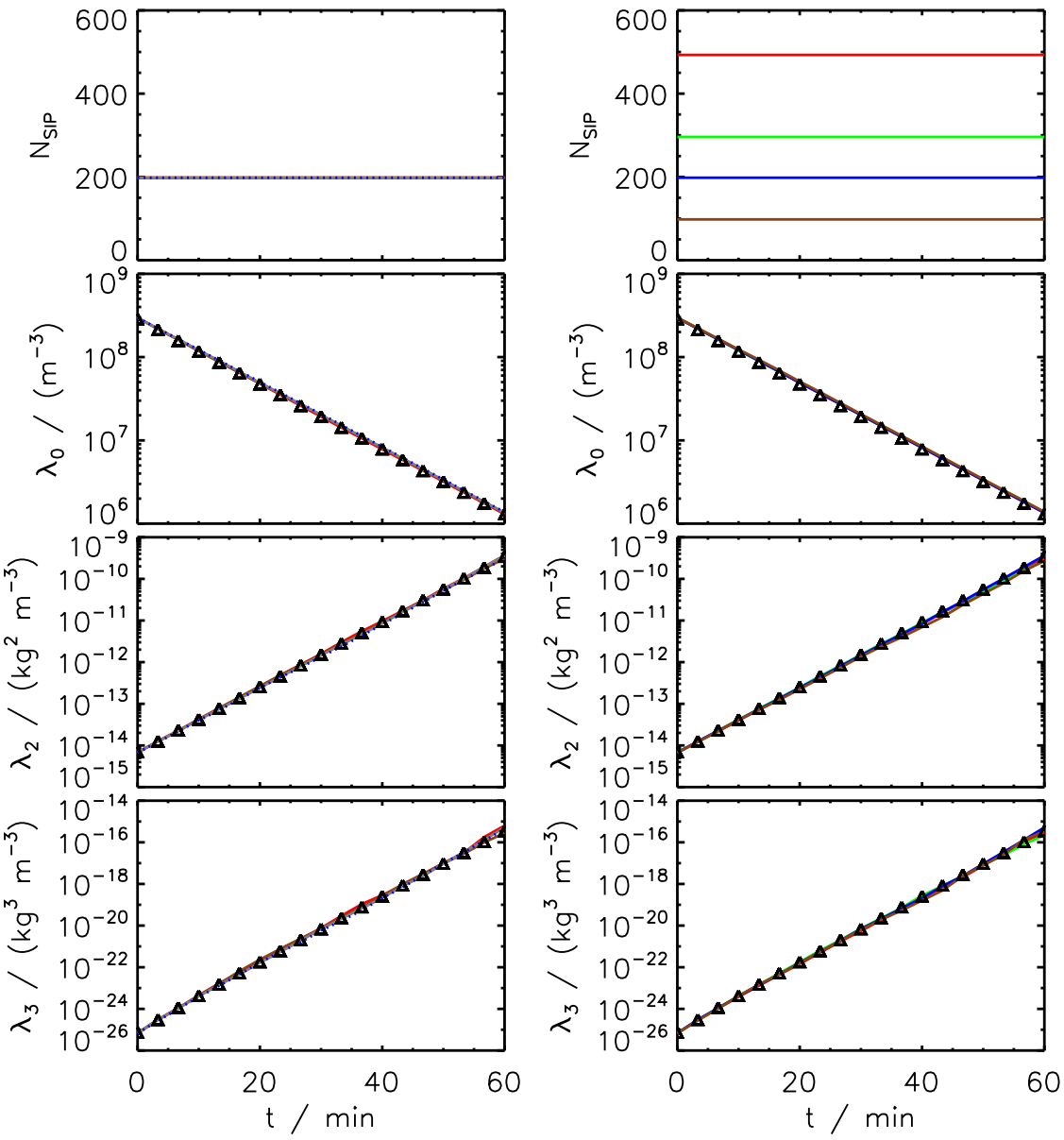

Figure 27: GOL AON: Variation of time step dt (left) and bin resolution κ (right).

4.1.4 Golovin Kernel (AON), ν_{const}-init

4.1.4.1 Variation of dt and N_{SIP}

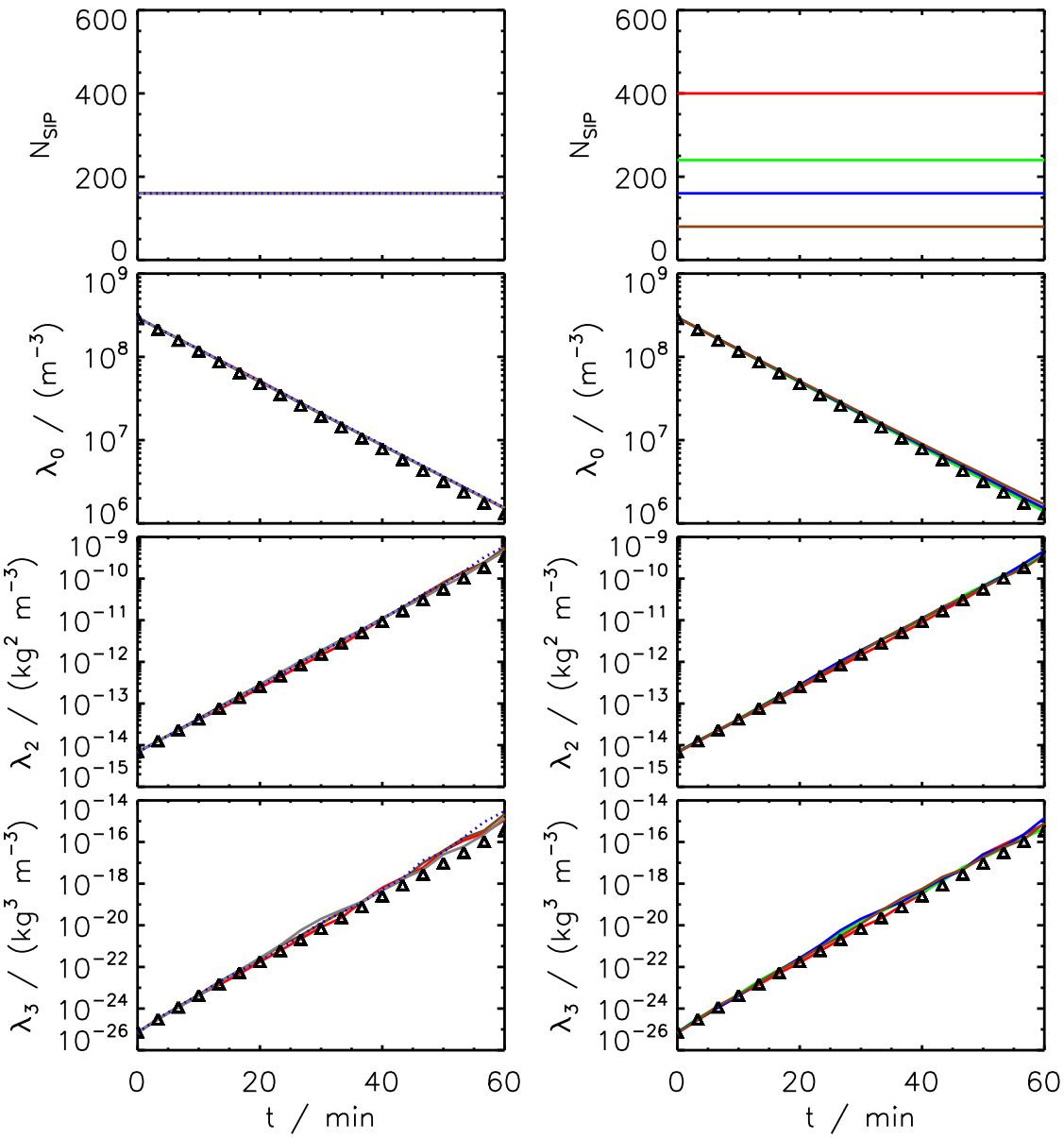

Figure 28: GOL AON: Variation of time step dt and SIP number N_{SIP}.

4.1.5 Golovin Kernel (AON), ν_{draw}-init

4.1.5.1 Variation of dt and N_{SIP}

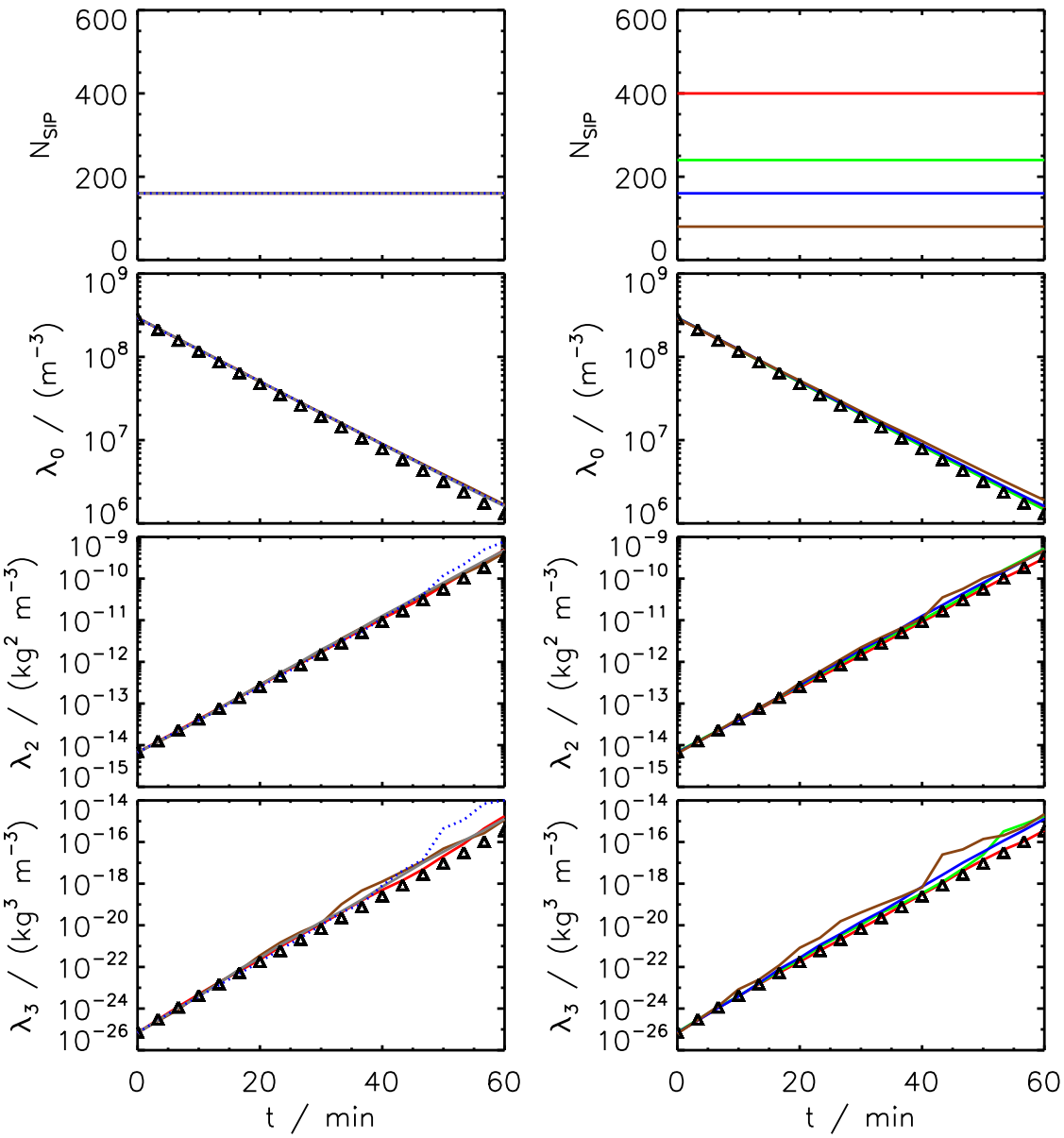

Figure 29: GOL AON: Variation of time step dt and SIP number N_{SIP}.

4.2 Long Kernel (AON)

The following sections show Long AON results for six types of init methods.

4.2.1 Long Kernel (AON), SingleSIP-init

4.2.1.1 Variation of dt and κ

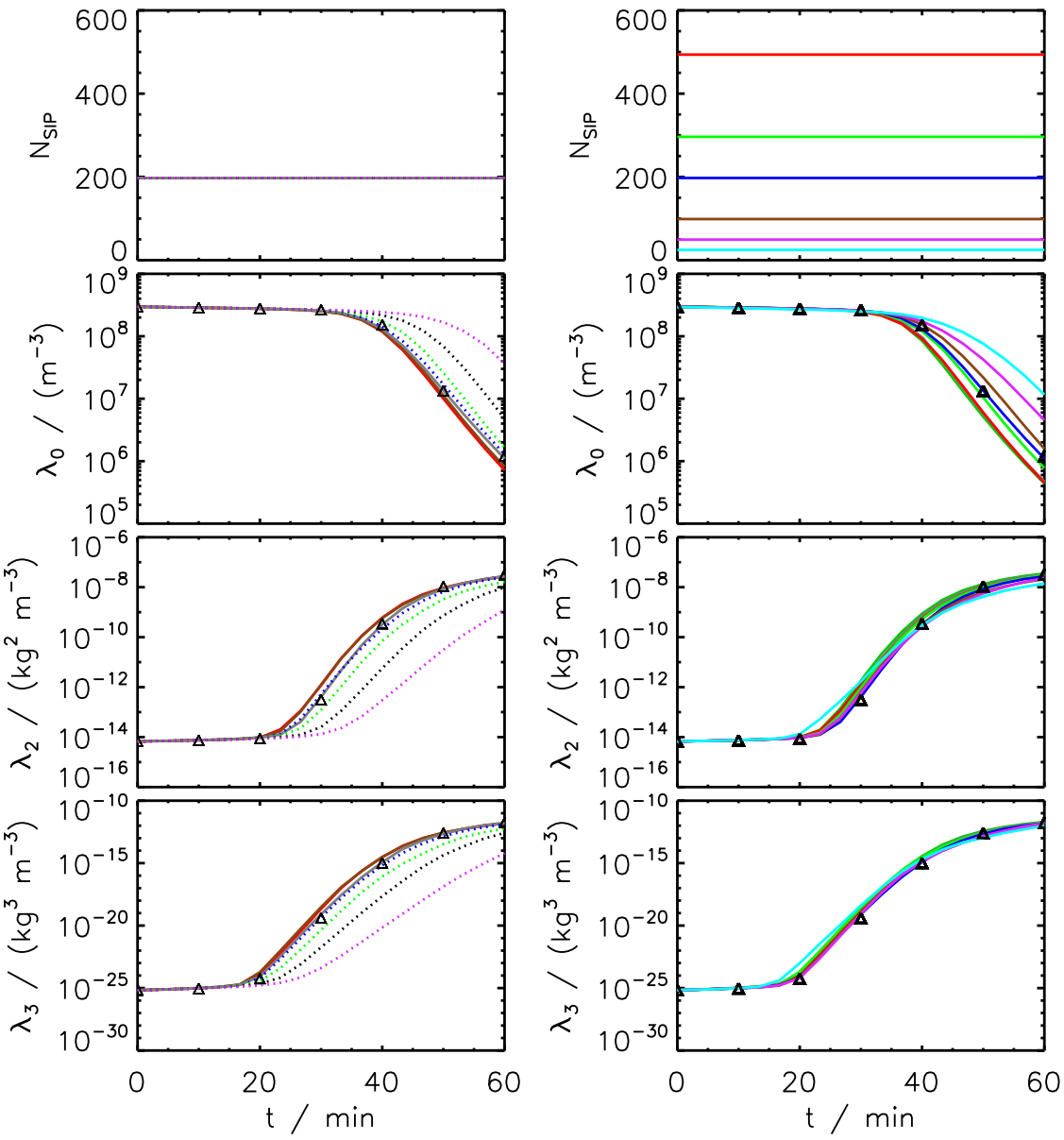

Figure 30: LONG AON: Variation of time step dt (left) and bin resolution κ (right).

4.2.1.2 Variation of η

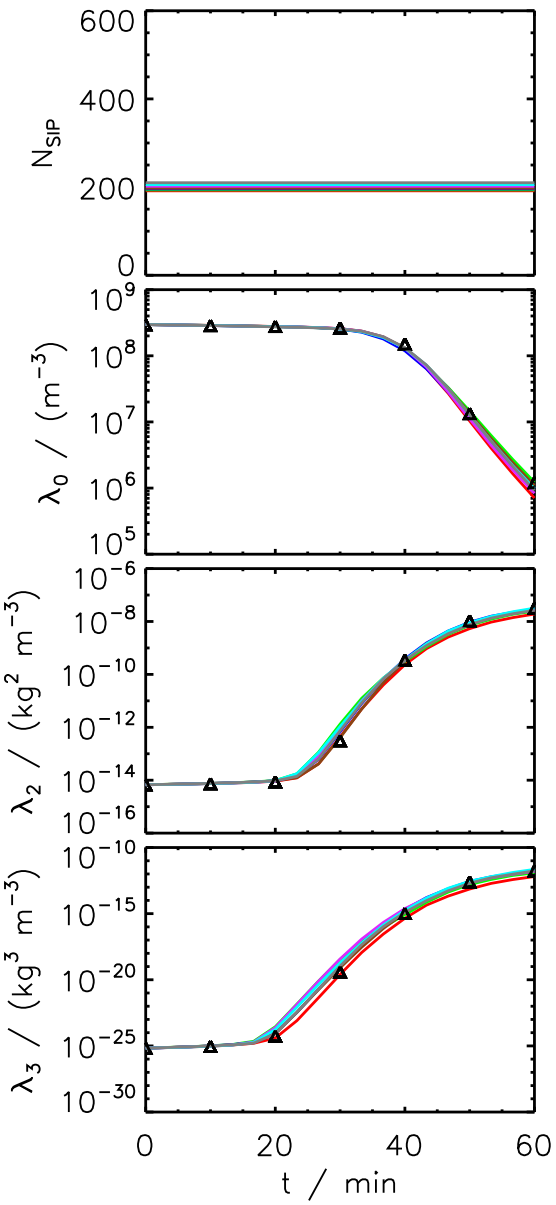

Figure 31: LONG AON: Variation of threshold η.

4.2.1.3 No multiple collections

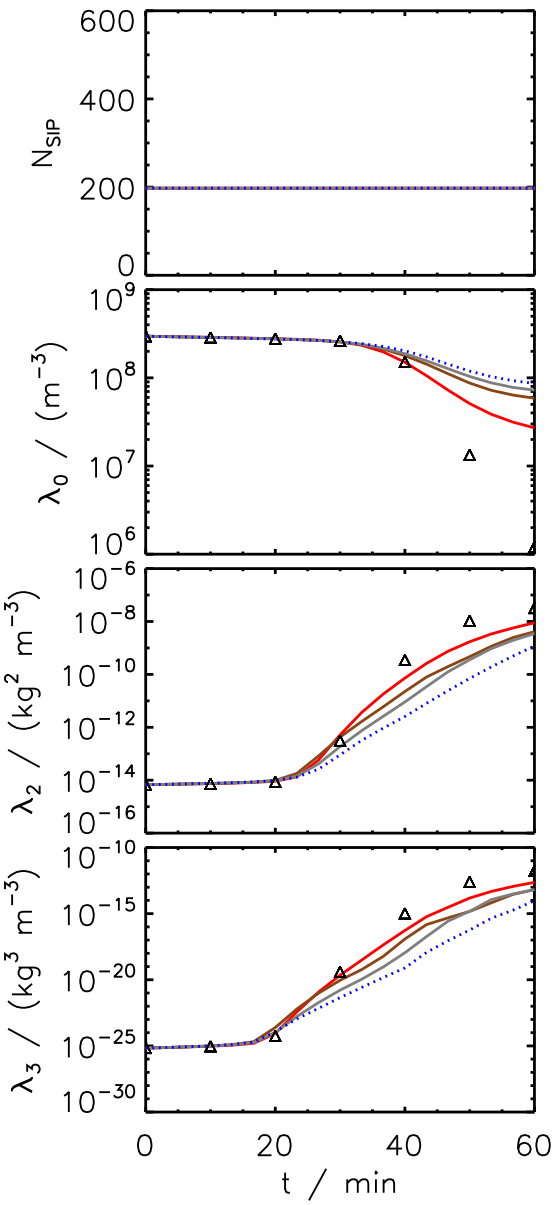

Figure 32: LONG AON: Variation of time step *dt*.

4.2.1.4 Variation of $r_{critmin}$

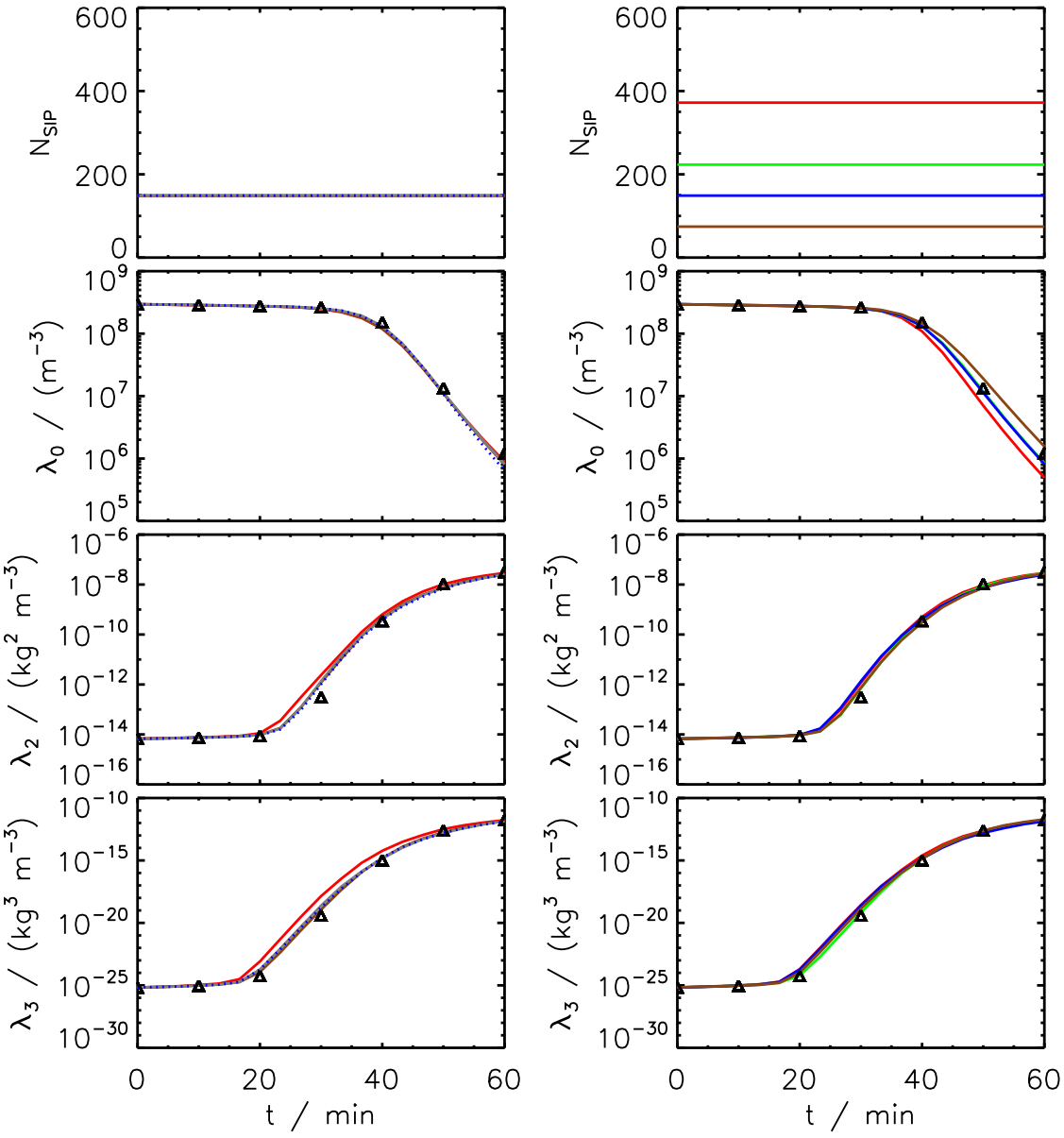

Figure 33: LONG AON: Variation of time step dt (left) and bin resolution κ (right) at $r_{critmin} = 1.6\,\mu$m.

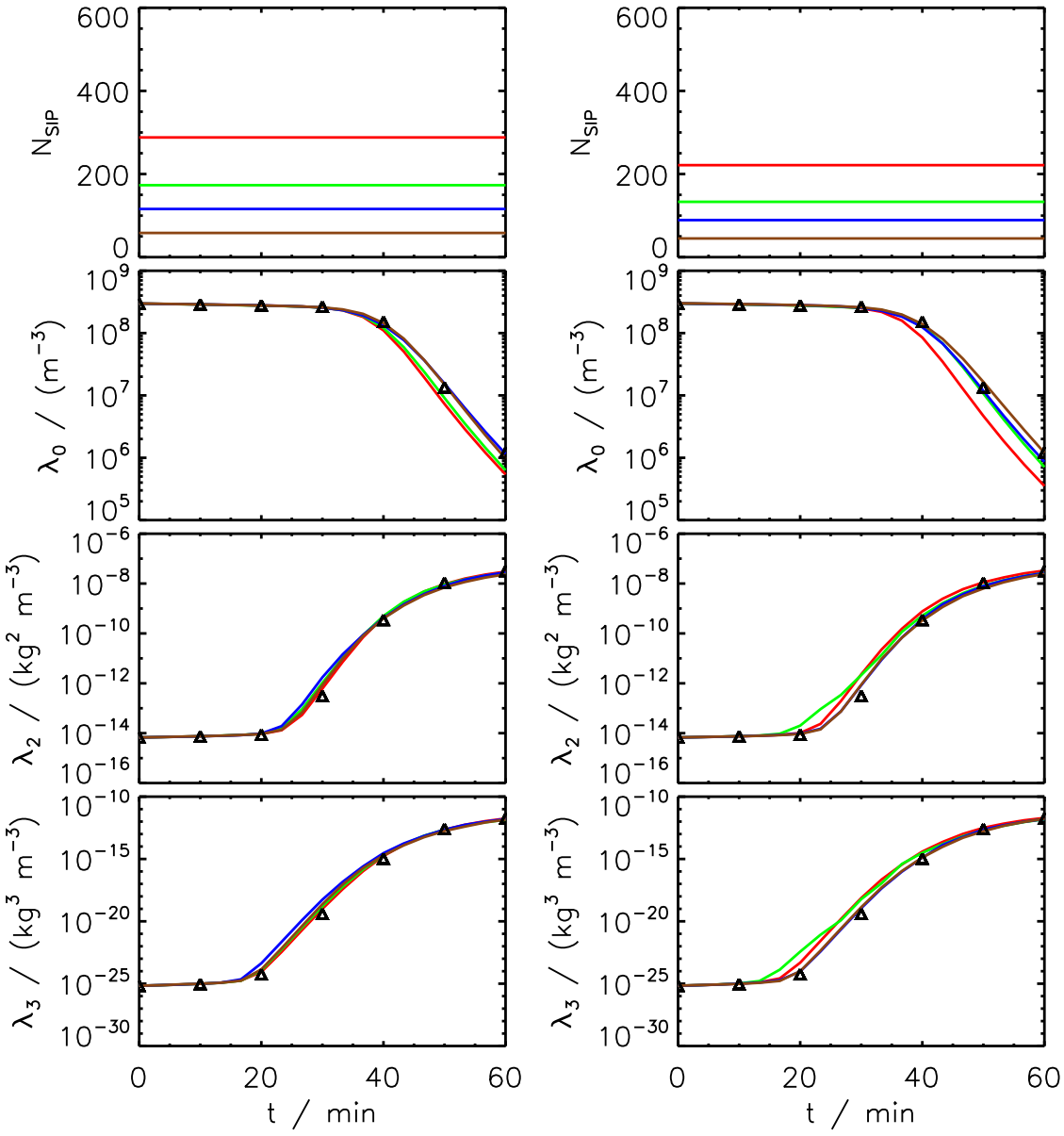

Figure 34: LONG AON: Variation of bin resolution κ at $r_{critmin} = 3.0\,\mu$m (left) and $5.0\,\mu$m (right).

4.2.1.5 Variation of t_{init}

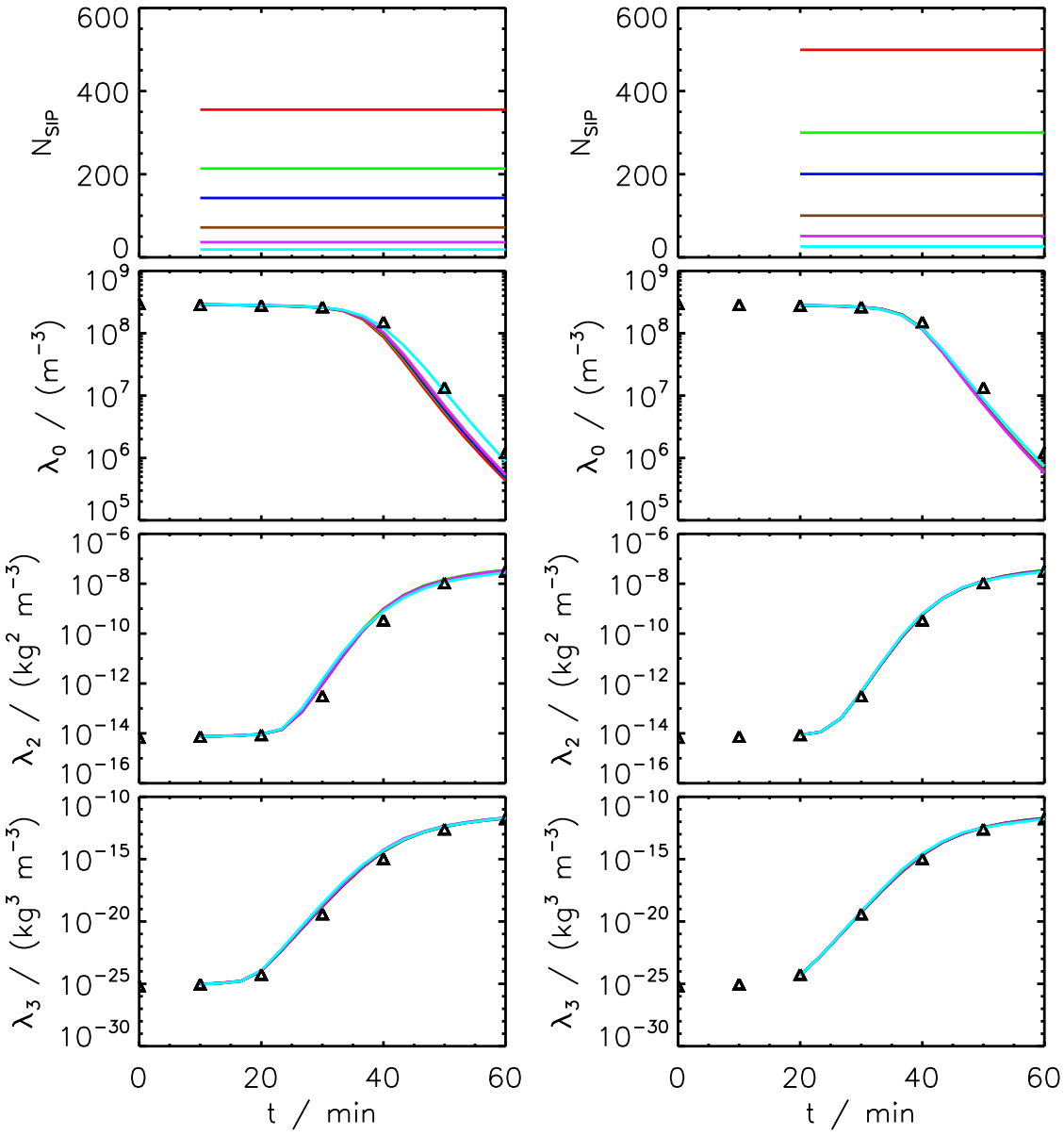

Figure 35: LONG AON: Variation of bin resolution κ at $t_{init} = 10\,\text{min}$ (left) and $20\,\text{min}$ (right).

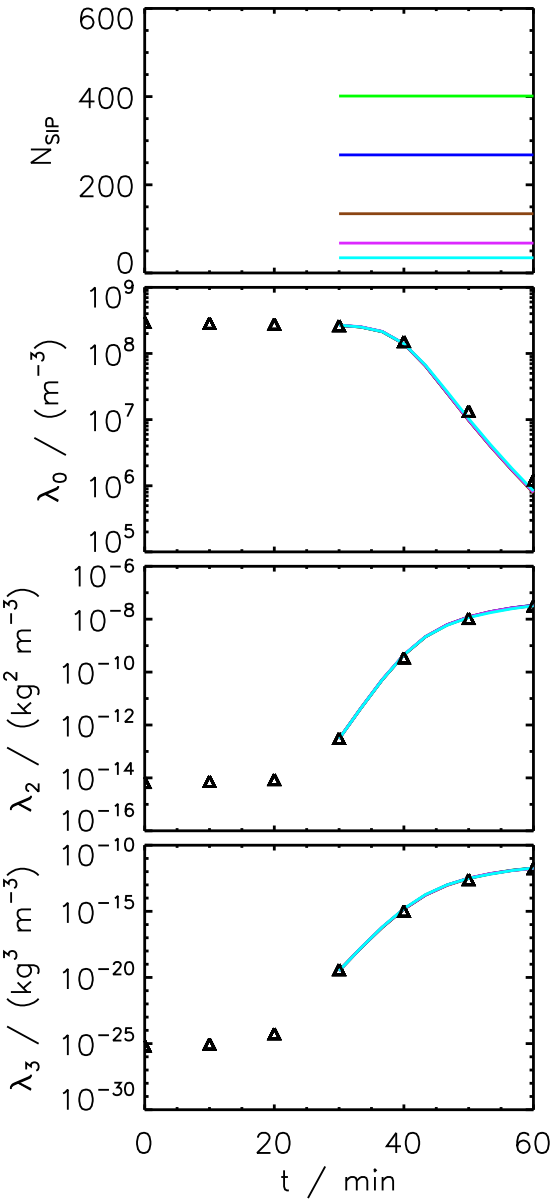

Figure 36: LONG AON: Variation of bin resolution κ at $t_{init} = 30\,\text{min}$.

4.2.1.6 Order of combination processing The AON algorithm is inherently updating the SIP weights on the fly. Then, the results may depend on the order the SIP combinations are processed. As default, the algorithm starts with combinations of the smallest SIPs. The version OTF$_l$ first treats the largest SIPs, the RANDorder version uses in each time iteration a randomly chosen order.

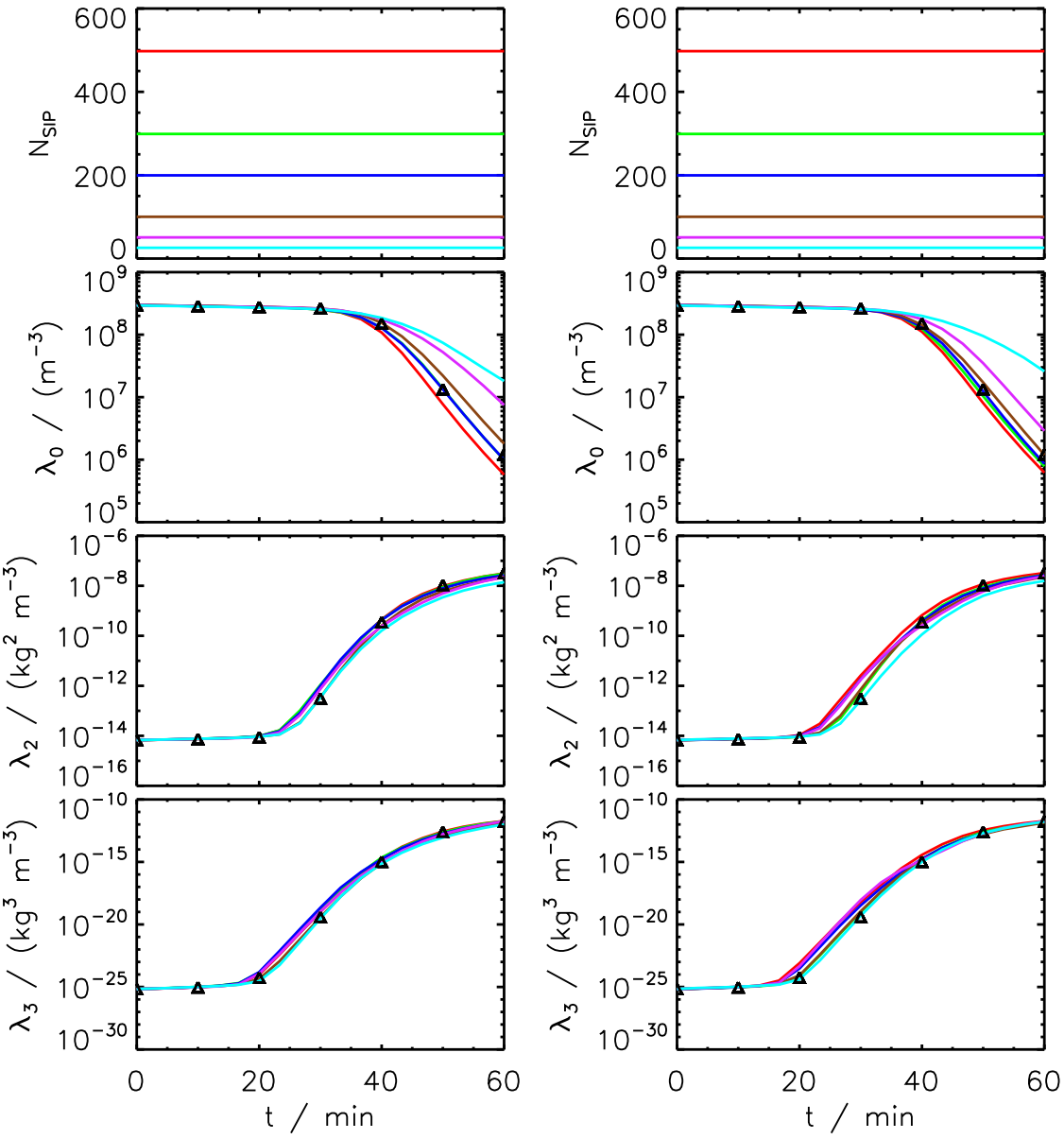

Figure 37: LONG AON: Variation of bin resolution κ OTF$_l$ (left) and RANDorder (right)

4.2.1.7 Hybrid init The radius spectrum is divided into two parts. For radii $r > 16\,\mu$m, a high resolution with $\kappa_{high} = 100$ is used irrespetive of the chosen κ. For smaller radii, the chosen κ is used.

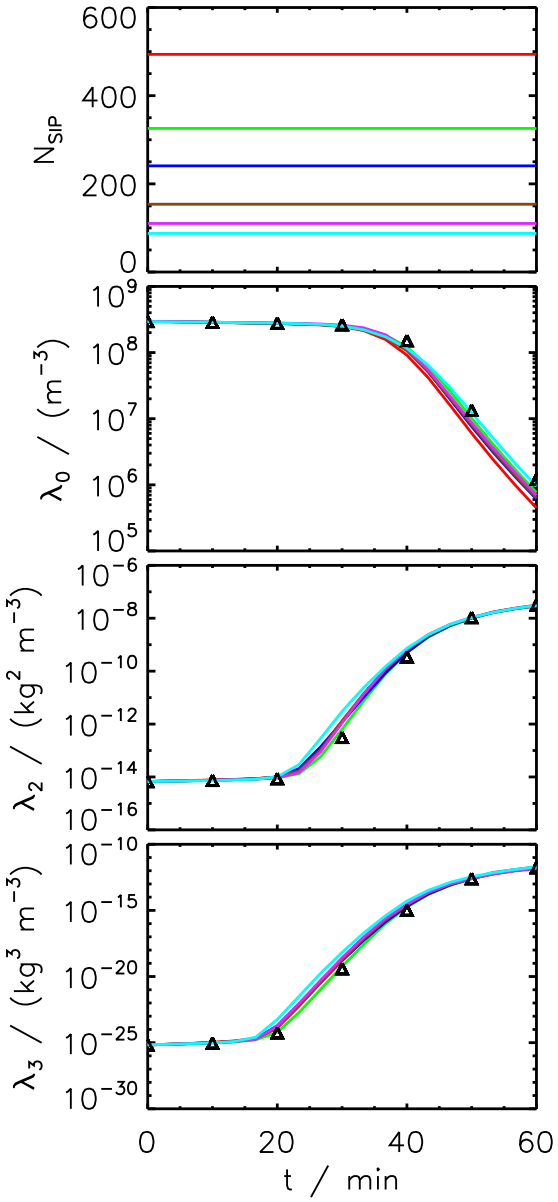

Figure 38: LONG AON: Variation of bin resolution κ (for $r < 16\,\mu$m). For $r > 16\,\mu$m, $\kappa_{high} = 100$ is used.

4.2.2 Long Kernel (AON), MultiSIP-init

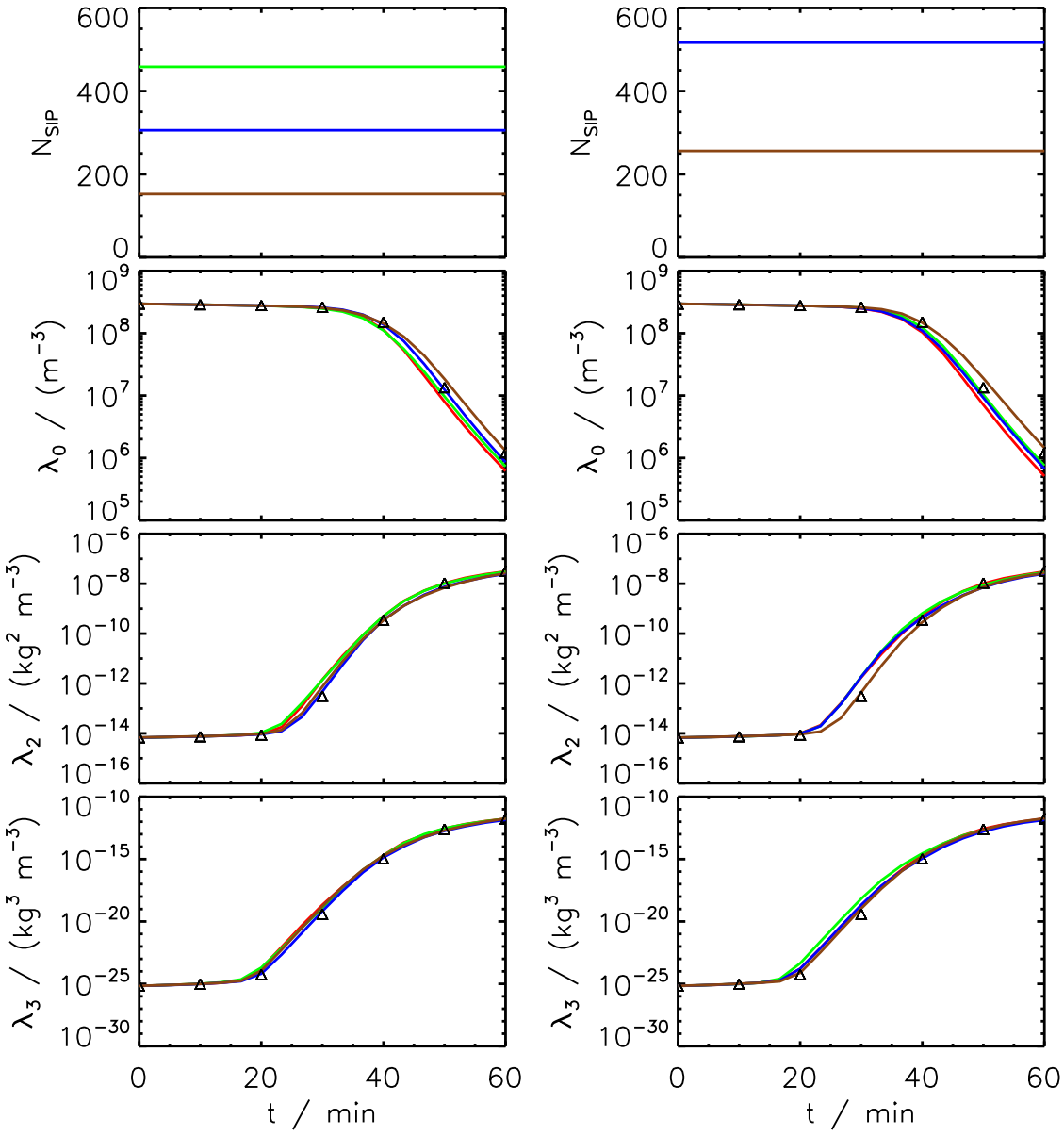

Figure 39: LONG AON: Variation of bin resolution κ for $\nu_{critmax} = 0.2 \cdot \max \nu_b$ (left) and $\nu_{critmax} = 0.1 \cdot \max \nu_b$ (right).

4.2.3 Long Kernel (AON), ν_{const}-init

For collections with $\nu_i = \nu_j$, $\xi = 0.5$.

4.2.3.1 Variation of dt and N_{SIP}

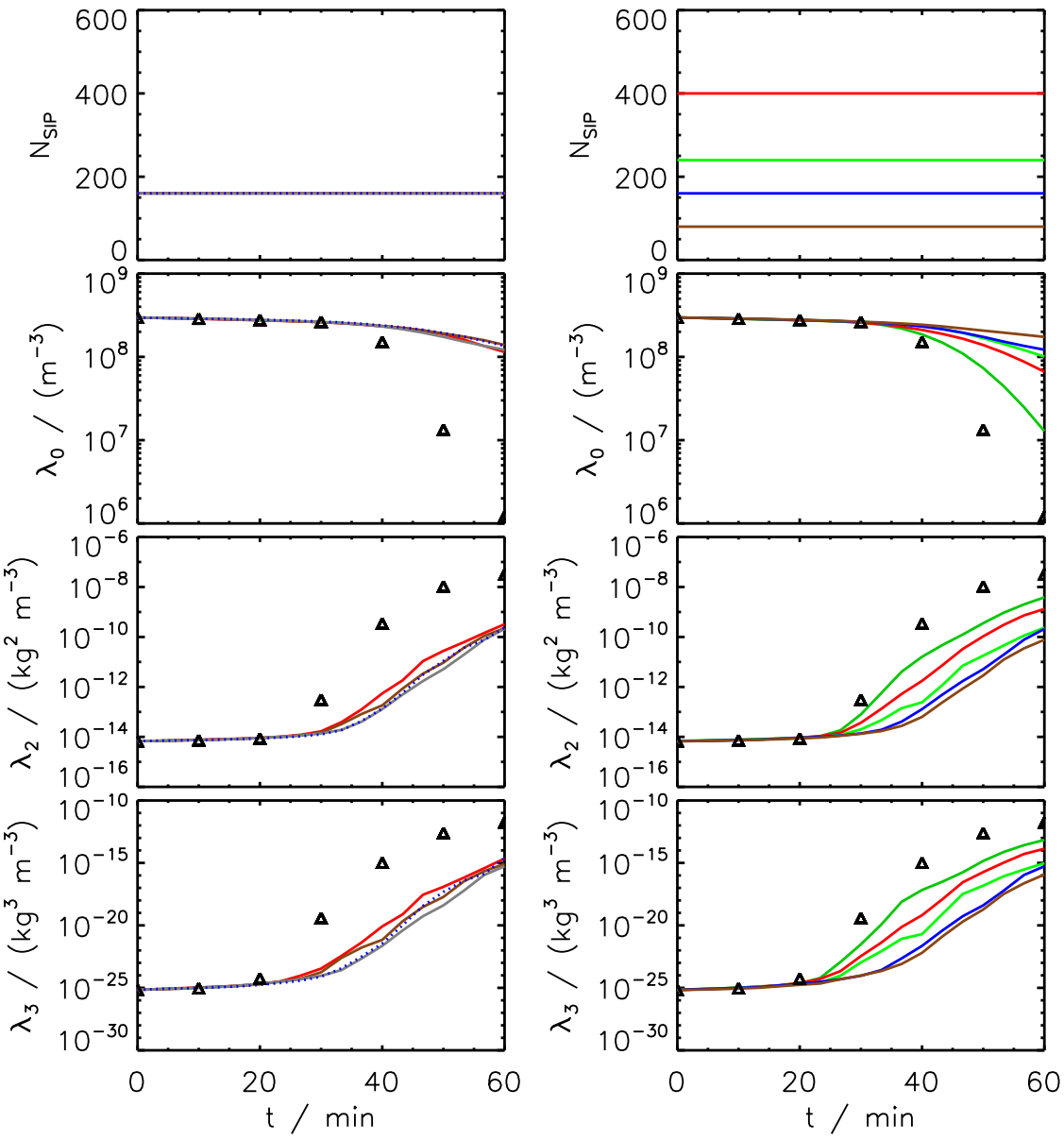

Figure 40: LONG AON: Variation of time step dt and SIP number N_{SIP}.

4.2.4 Long Kernel (AON), ν_{const}-init, randlin ξ

For collections with $\nu_i = \nu_j$, ξ =rand(), where rand() generates uniformly distributed random numbers from 0 to 1.

4.2.4.1 Variation of dt and N_{SIP}

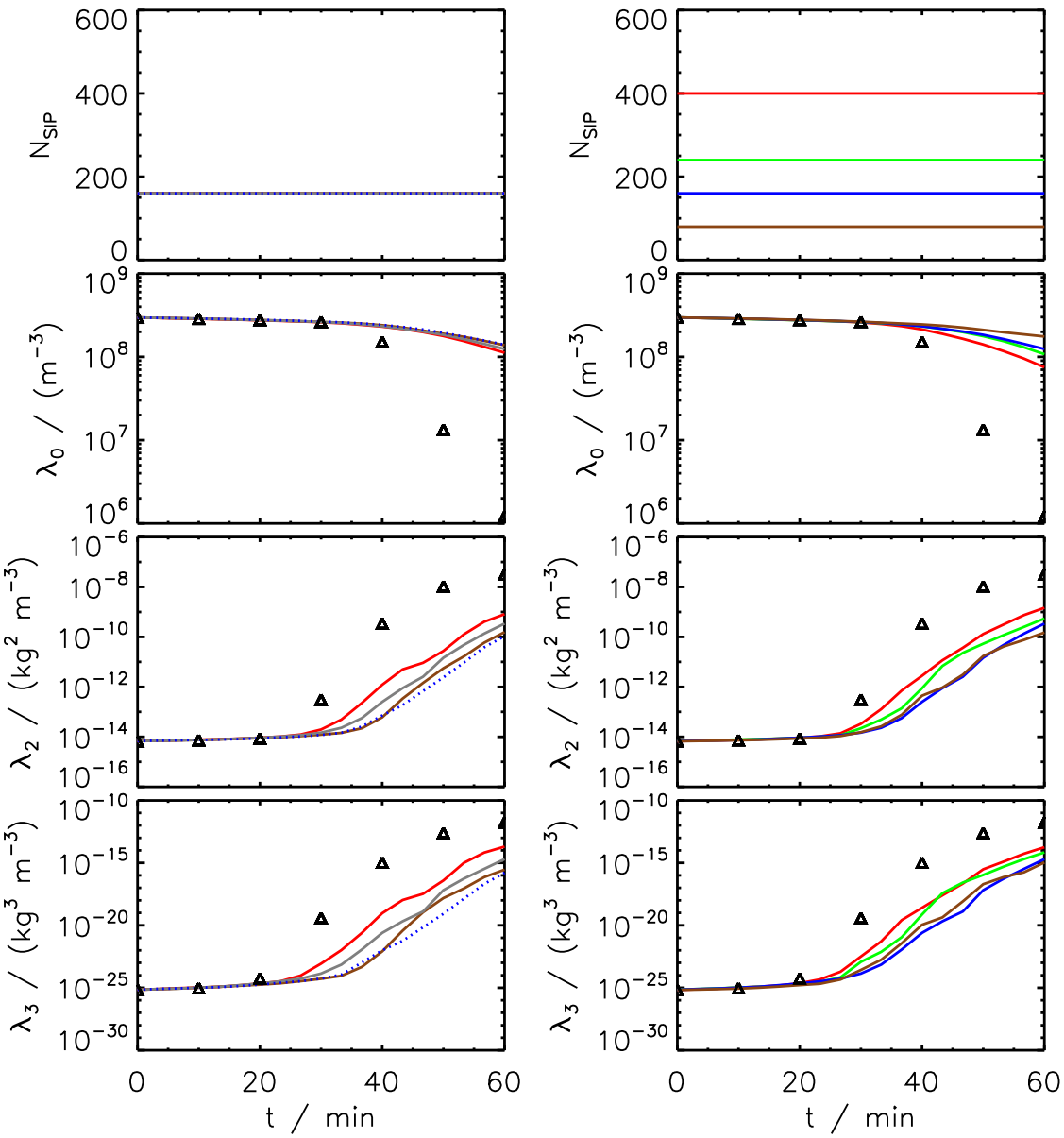

Figure 41: LONG AON: Variation of time step dt and SIP number N_{SIP}.

4.2.5 Long Kernel (AON), ν_{const}-init, randlog ξ

For collections with $\nu_i = \nu_j$, $\xi = 10^{-10\,\mathrm{rand}()}$, where rand() generates uniformly distributed random numbers from 0 to 1.

4.2.5.1 Variation of dt and N_{SIP}

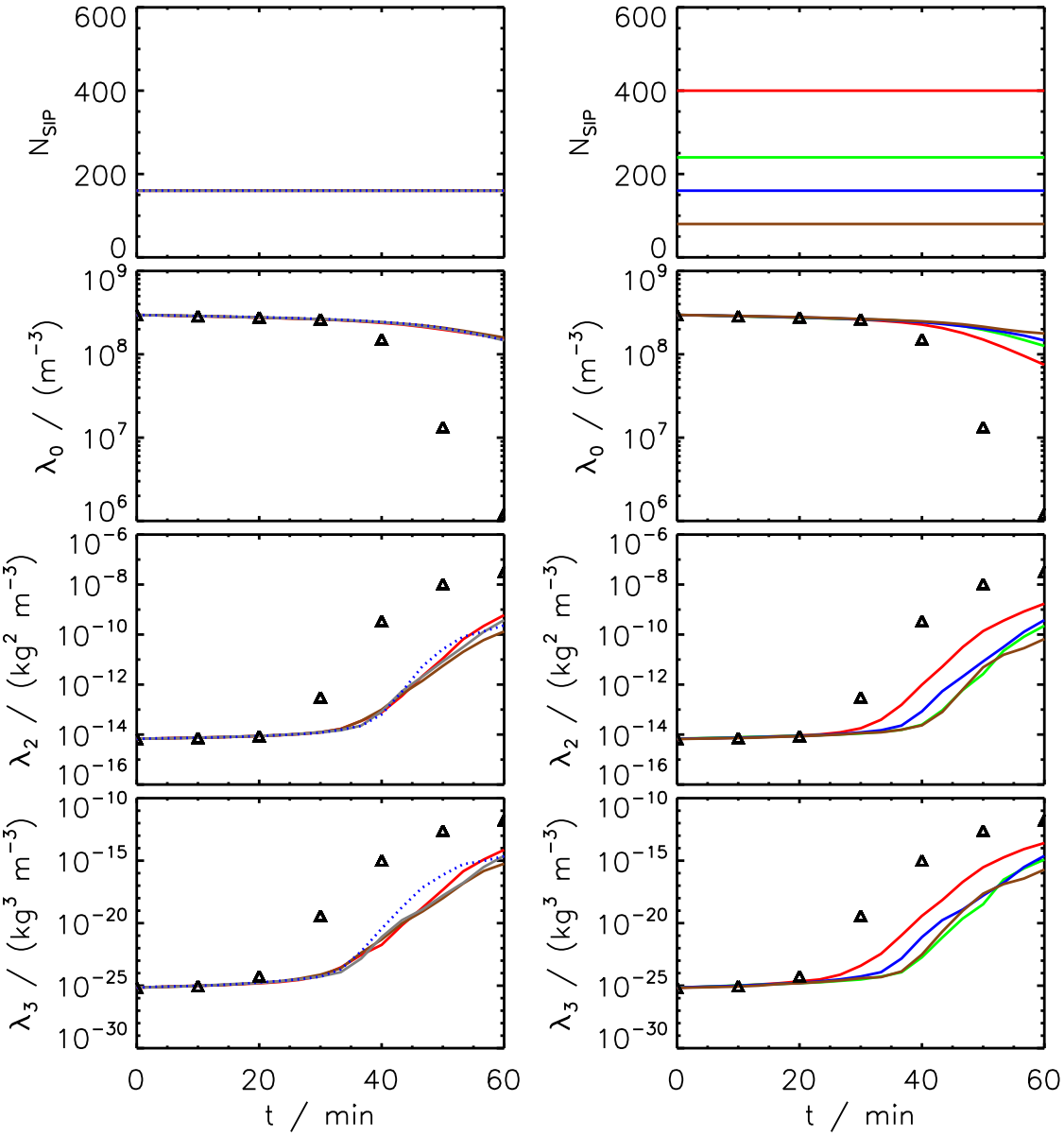

Figure 42: LONG AON: Variation of time step dt and SIP number N_{SIP}.

4.2.6 Long Kernel (AON), ν_{const}-init, randlog ξ v2

For collections with $\nu_i = \nu_j$, $\xi = 10^{-10\,\mathrm{rand}()^2}$, where rand() generates uniformly distributed random numbers from 0 to 1.

4.2.6.1 Variation of dt and N_{SIP}

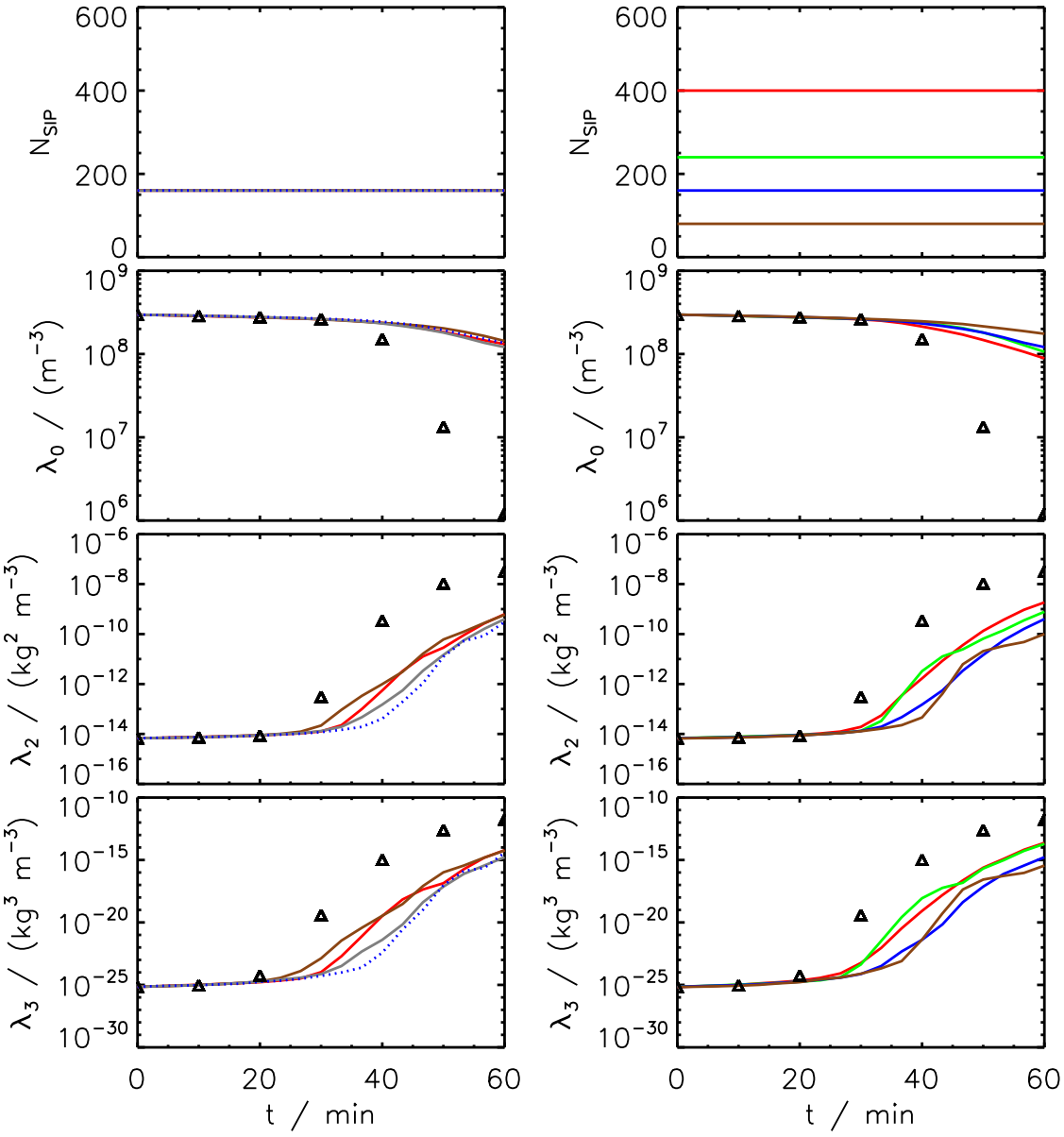

Figure 43: LONG AON: Variation of time step dt and SIP number N_{SIP}.

4.2.7 Long Kernel (AON), ν_{draw}-init

4.2.7.1 Variation of dt and N_{SIP}

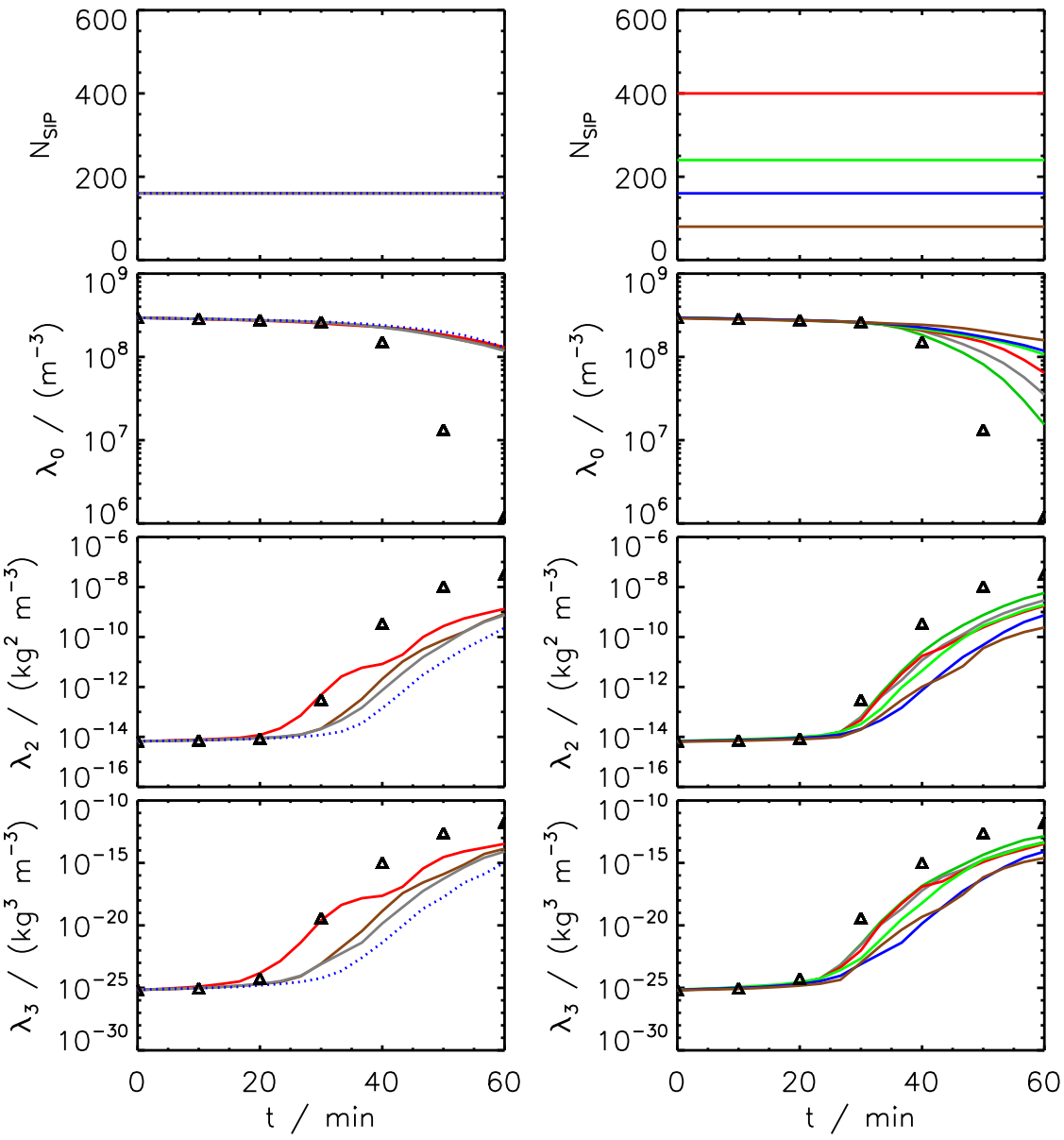

Figure 44: LONG AON: Variation of time step dt and SIP number N_{SIP}.

4.2.8 Long Kernel (AON), $\nu_{random,rs}$-init

4.2.8.1 Variation of dt and α_{low}

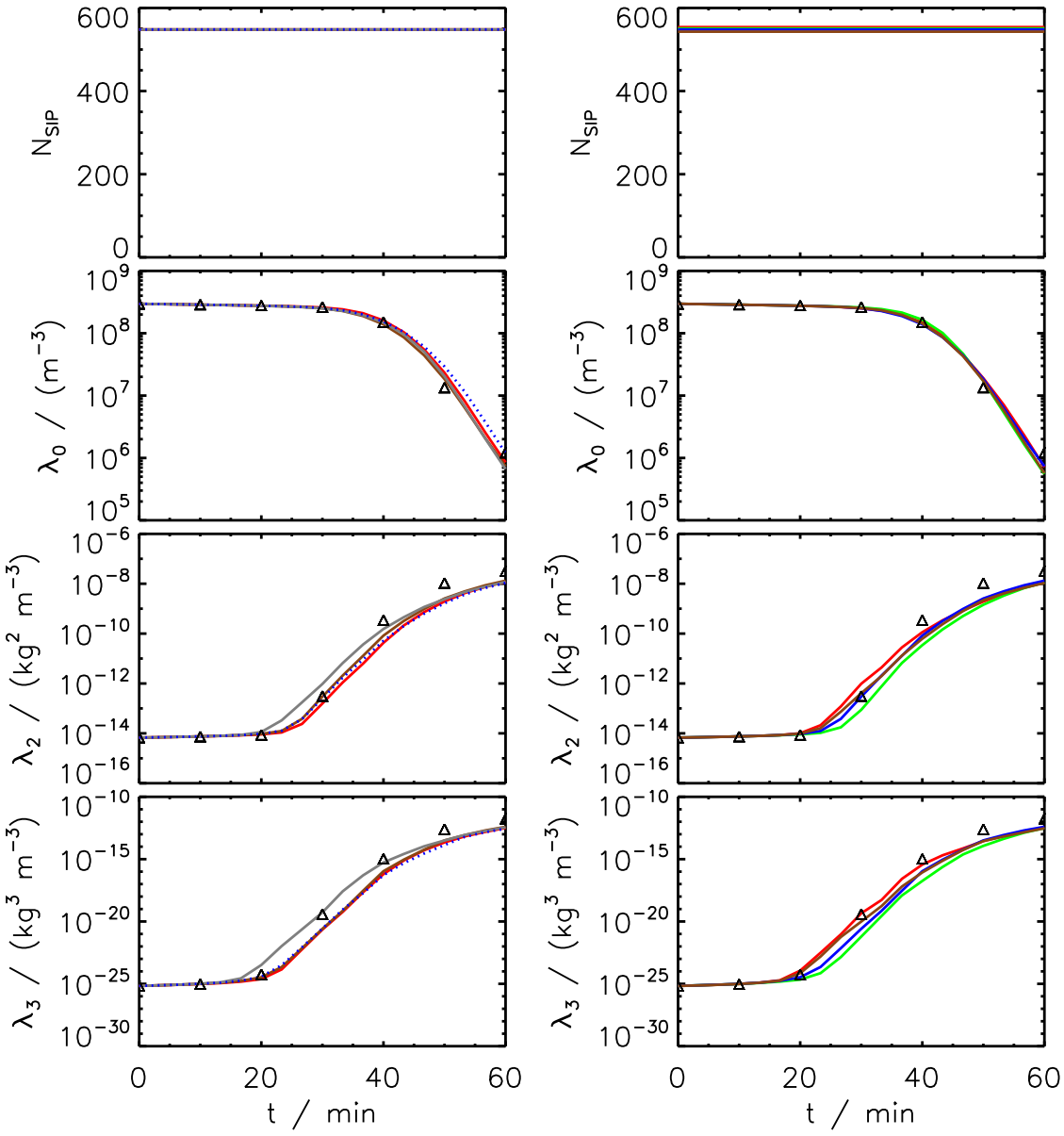

Figure 45: LONG AIM: Variation of time step dt (left) and lower threshold α_{low} (right, at $dt = 5\,\mathrm{s}$).

4.2.9 Long Kernel (AON), $\nu_{random,lb}$-init

4.2.9.1 Variation of dt and α_{low}

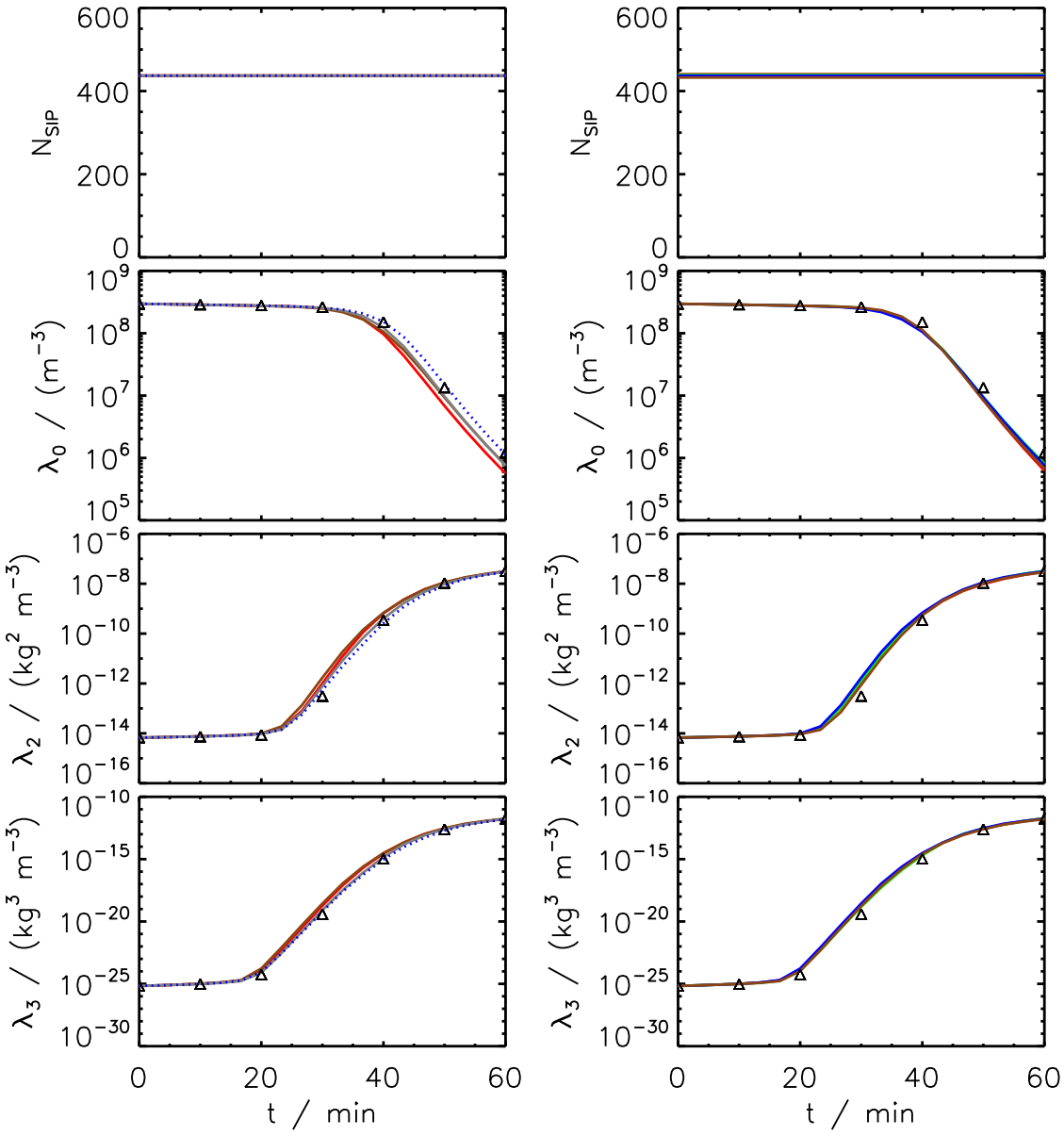

Figure 46: LONG AIM: Variation of time step dt (left) and lower threshold α_{low} (right, at $dt = 5\,\mathrm{s}$).

4.3 Hall Kernel (AON)

The following sections show Long AON results for three types of init methods.

4.3.1 Hall Kernel (AON), SingleSIP-init

4.3.1.1 Variation of dt and κ

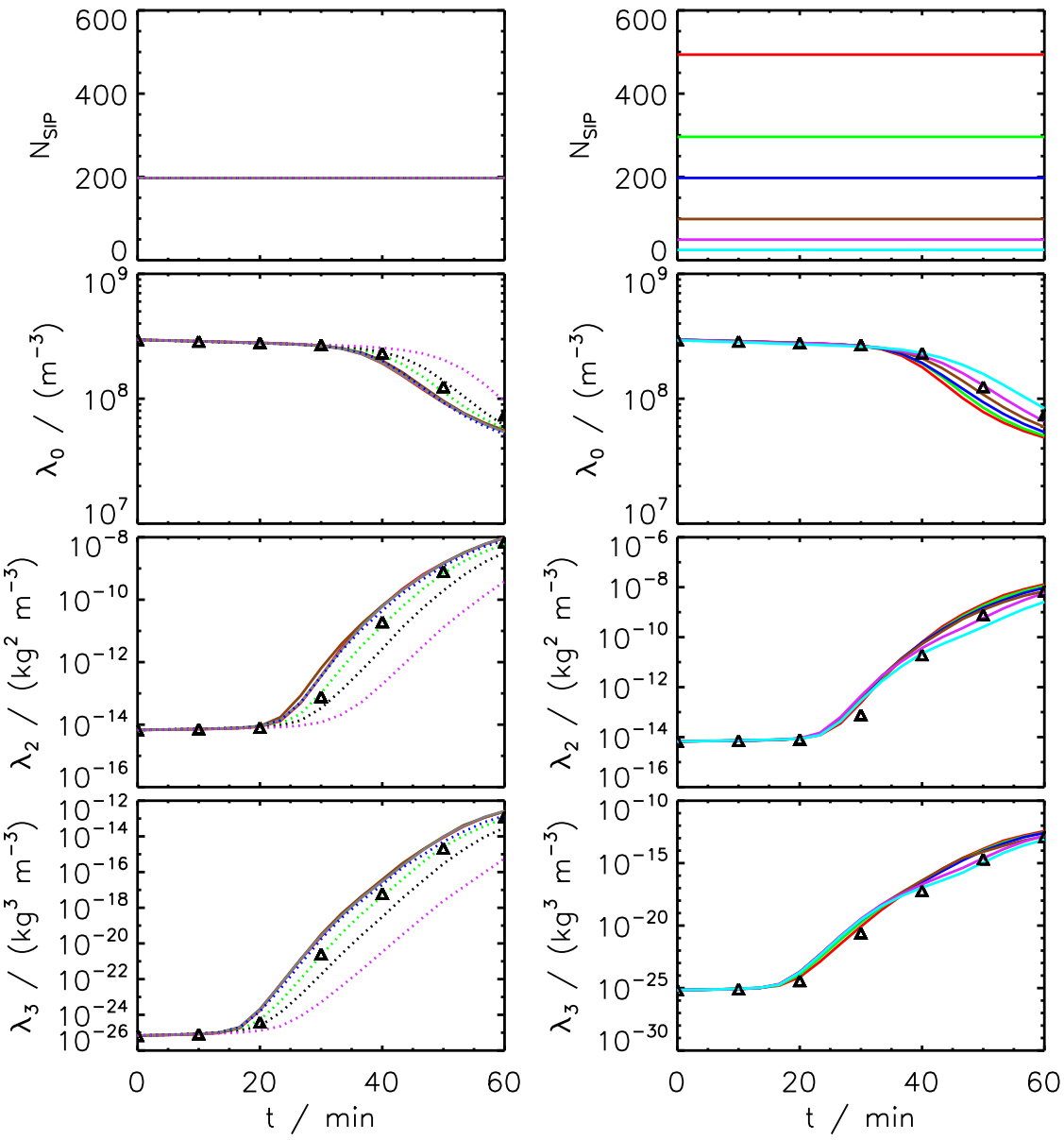

Figure 47: HALL AON: Variation of time step dt (left) and bin resolution κ (right).

4.3.1.2 Variation of η

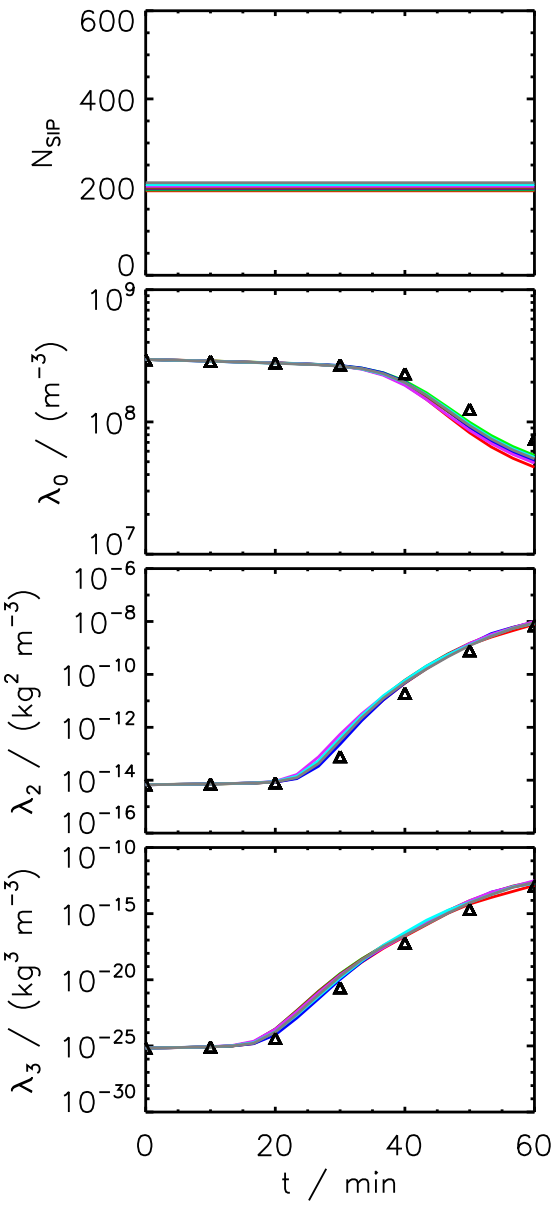

Figure 48: HALL AON: Variation of threshold η.

4.3.1.3 Variation of $r_{critmin}$

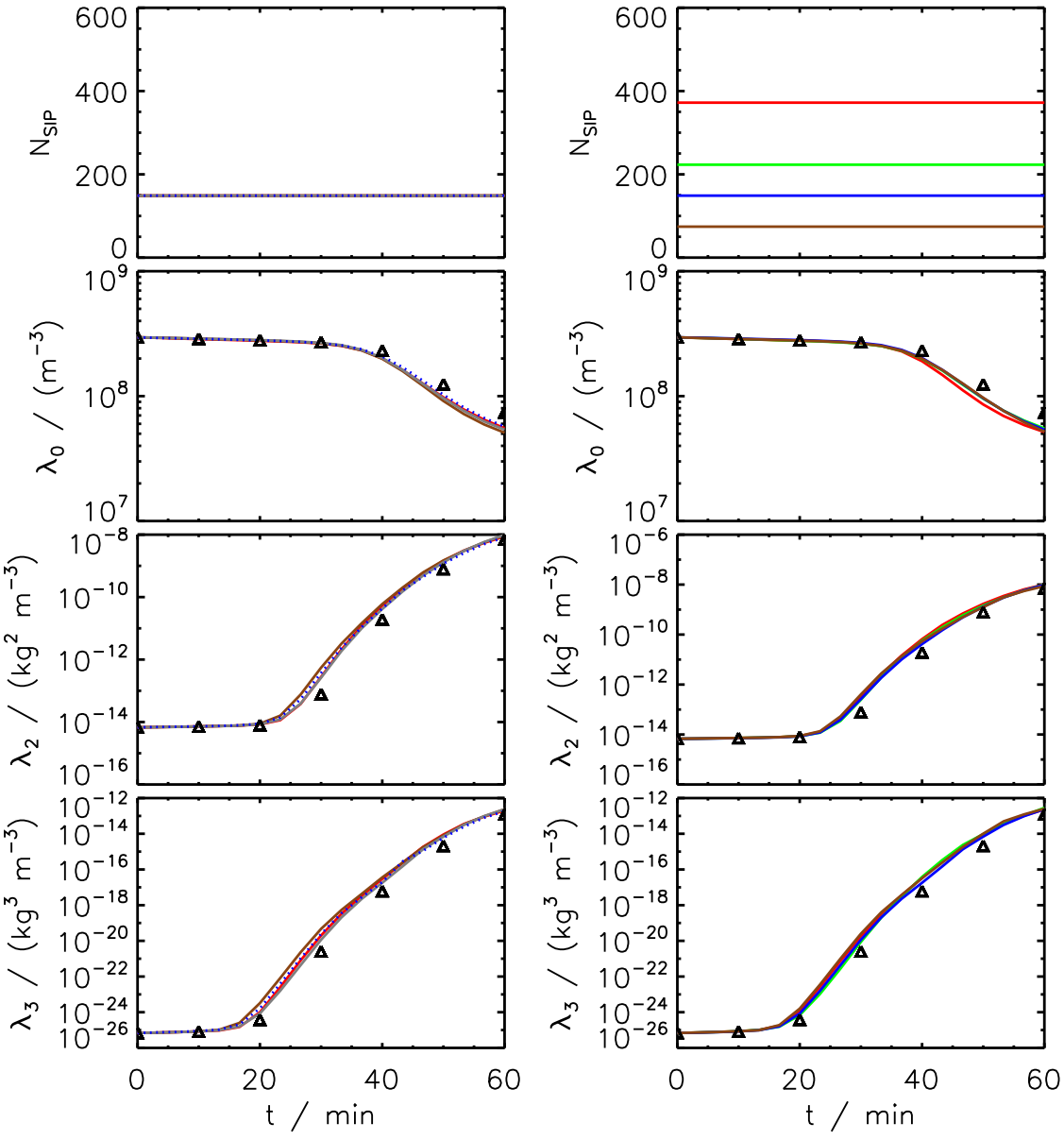

Figure 49: HALL AON: Variation of of time step dt (left) and bin resolution κ (right) at $r_{critmin} = 1.6\,\mu$m.

4.3.2 Hall Kernel (AON), ν_{const}-init

4.3.2.1 Variation of dt and N_{SIP}

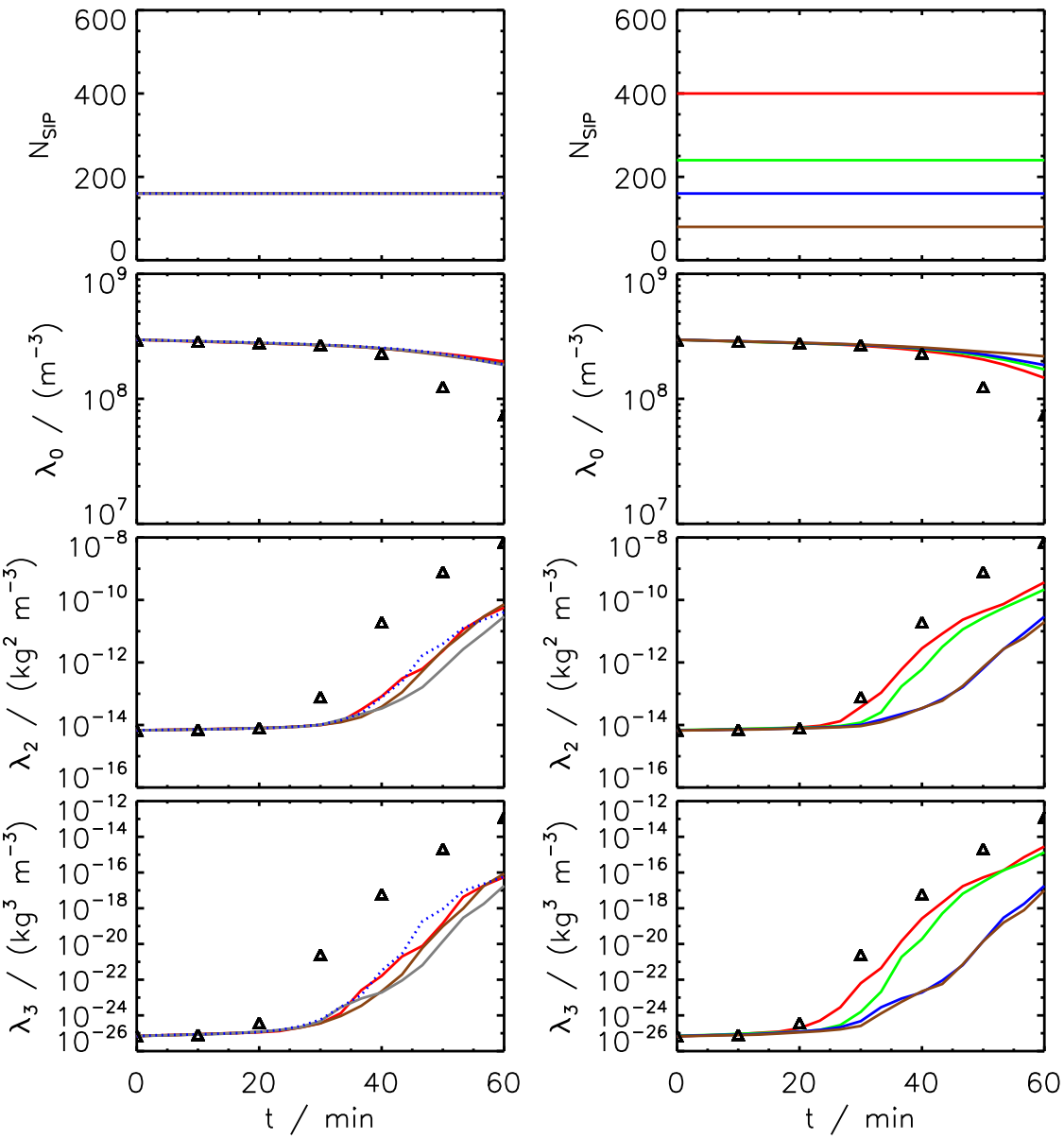

Figure 50: HALL AON: Variation of time step dt and SIP number N_{SIP}.

4.3.3 Hall Kernel (AON), ν_{draw}-init

4.3.3.1 Variation of dt and N_{SIP}

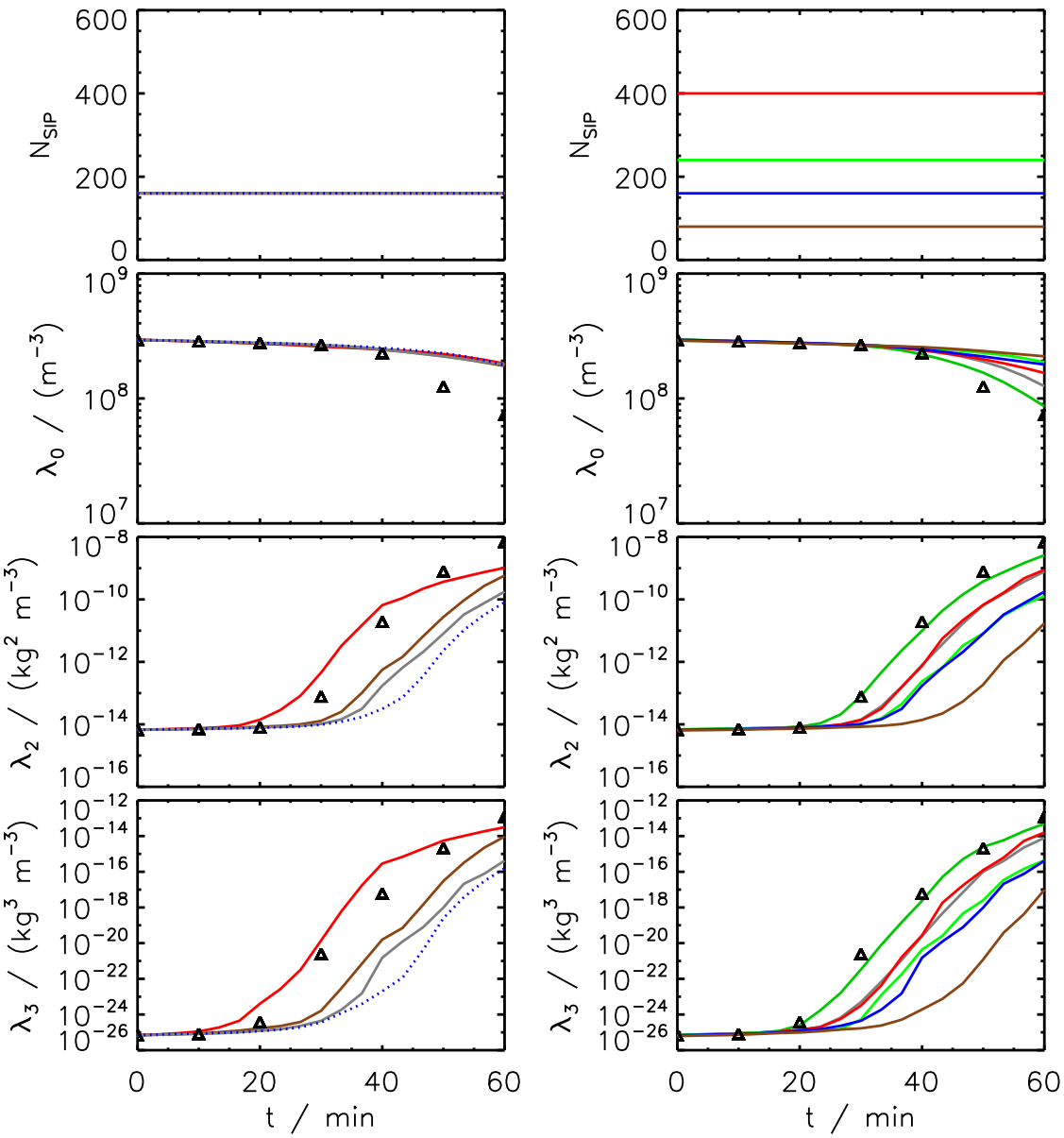

Figure 51: HALL AON: Variation of time step dt and SIP number N_{SIP}.

4.4 Constant efficiency Kernel (AON)

This subsection shows simulations for a hydrodynamic kernel with constant efficiency E_c, which is assigned a value of 1.0 or 0.2.

4.4.1 Collection efficiency $E_c = 0.2$, SingleSIP-init

4.4.1.1 Variation of dt and κ

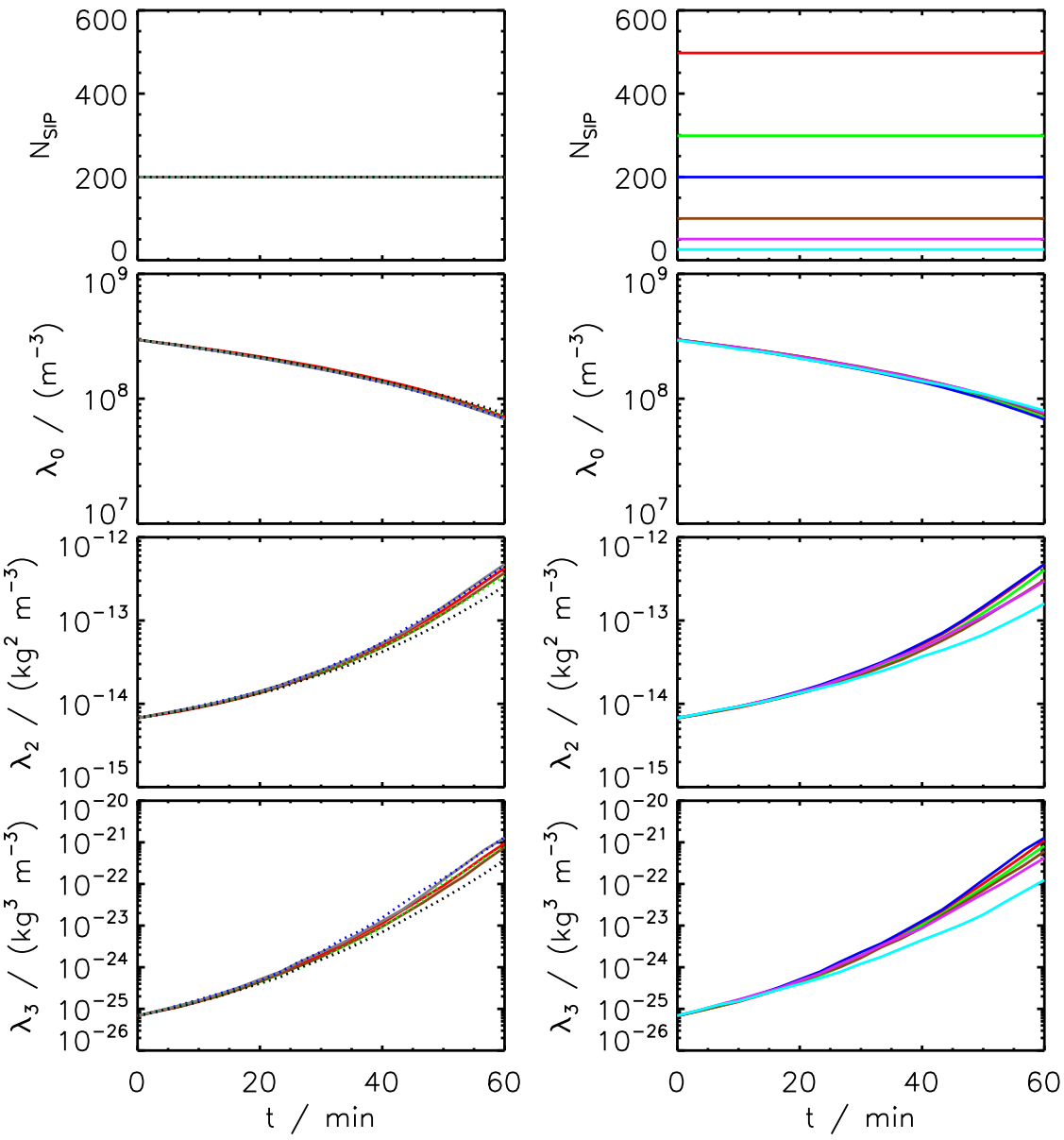

Figure 52: EC=0.2 AON: Variation of time step dt (left) and bin resolution κ (right).

4.4.2 Collection efficiency $E_c = 1.0$, SingleSIP-init

4.4.2.1 Variation of κ

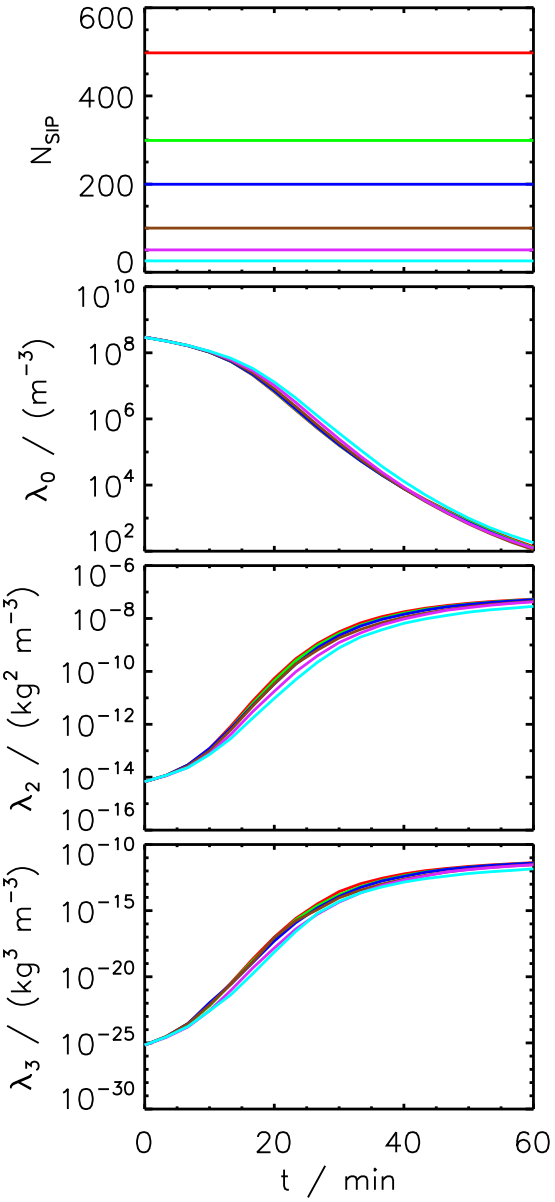

Figure 53: EC=1.0 AON: Variation of bin resolution κ.